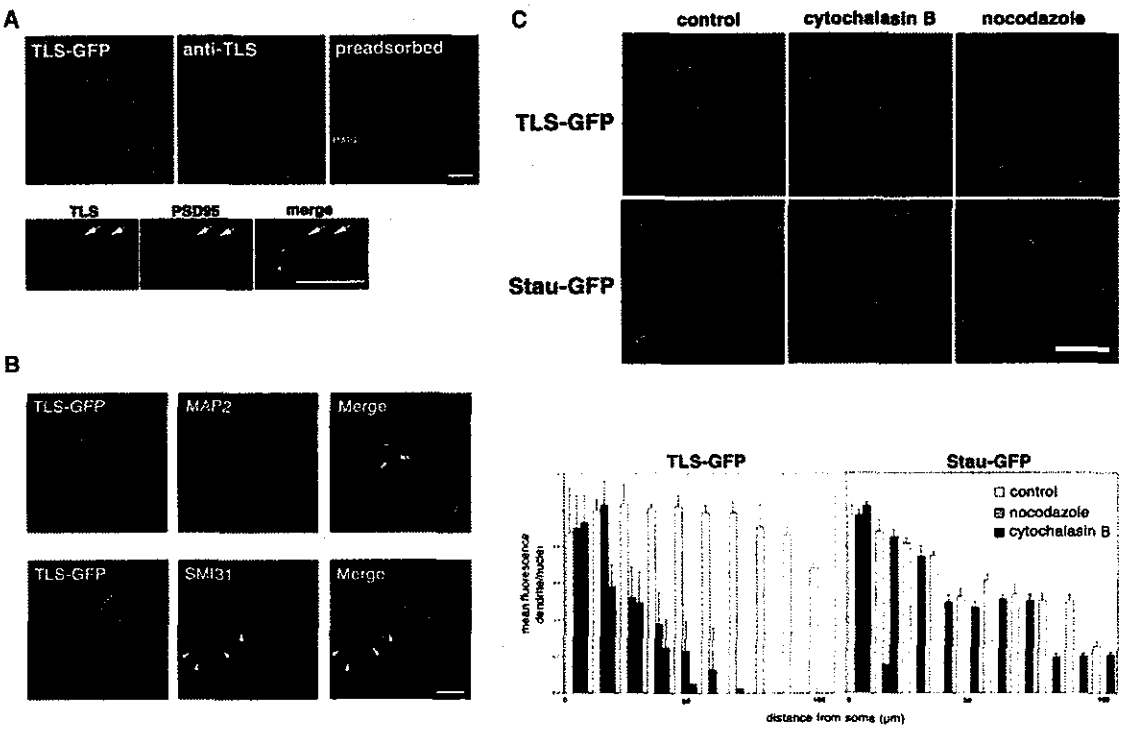

Figure 1. TLS Is Localized in Neuronal Dendrites

(A) Immunocytochemistry of mouse hippocampal-cultured neurons shows a punctate distribution of TLS within dendrites and its clustering in the nucleus (top middle). No staining with the antibody preadsorbed by excess amounts of GST-TLS fusion protein (top right, inset; costaining with anti-MAP2 antibody). Exogenously expressed TLS-GFP protein recapitulates the endogenous punctate localization of TLS within dendrites (top left). Double labeling with anti-PSD95 antibody shows that some of the TLS clusters are localized in spines (bottom arrows). Scale bars, 10 μm in upper panels and 5 μm in lower panels.

(B) TLS-GFP is localized in MAP2-positive neuronal dendrites, whereas TLS-GFP is absent in the MAP2-negative process (arrowheads). TLS-GFP is excluded from this SMI31-positive thin-axonal process (arrowheads) of a mouse hippocampal pyramidal neuron. Scale bars, 10 μm.

(C) TLS translocation to dendrites requires intact cytoskeletal polymers and is actin dependent. In control cells, TLS-GFP is distributed both in the cell bodies and dendrites (n = 27) as well as staufen-GFP. Treatment with either cytochalasin B (0.2 μM) (n = 48, over 50 μm distant from the soma, $p < 0.01$) or nocodazole (2 μM) (n = 51, over 70 μm distant from the soma, $p < 0.01$) for 12 hr reduces the amount of TLS-GFP within dendrites, although the neuronal extensions are not retracted. Nocodazole treatment blocks dendritic localization of staufen-GFP, however, cytochalasin B has no effect on its somatodendritic localization. *Scale bar, 50 μm. Graphs showing* quantitative data for pharamacological experiments with inhibitors described above are presented. Error bars indicate SEM (standard error of mean) for each experiment.

and 2). When TLS-GFP was expressed in immature dendrites with few spines (culture day 13, Figure 2A), rapid fusion (Figure 2A, 0–5 min, left arrows) and dissociation (Figure 2A, 0–5 min, right arrows) of a fraction of the TLS-GFP particles took place. Active movement of TLS-GFP particles over a short distance within dendrites was also observed (Figure 2A, 15–25 min, arrowhead). To measure the exchange rate of TLS-GFP molecules in the particles, we performed fluorescence recovery after photobleaching (FRAP) of TLS-GFP clusters present in dendrites. After photobleaching, fluorescent signals of TLS-GFP were recovered rapidly, and half recovery of fluorescence was observed within 20 s (data not shown). This rapid time course of FRAP recovery indicates a dynamic exchange of TLS molecules between particulate and soluble fractions. The movement of TLS-GFP was also revealed to be bidirectional, and some populations of TLS-GFP particles formed stationary clusters within the dendritic shaft (Figures S1Ba–S1Bc). These clusters also repeatedly gathered and dispersed within the dendrites. By double labeling with anti-cortactin binding protein (CortBP), as an independent marker that identifies the morphology of the spines, and TLS-GFP, we further analyzed whether TLS-GFP clusters are localized in spines (Figure S2). The distribution of spines/filopodia labeled with anti-CortBP was different from that of TLS-GFP clusters, indicating that TLS is not selectively translocated into spines/filopodia at the early developmental stage. In mature dendrites at culture day 23, there was a significant shift of the localization of TLS-GFP particles from the dendritic shafts to spines (Figure 2B, arrow; see also Figure S1A and S1Ca–S1Cc), and these particles within the spines did not show the rapid movement that was evident in the immature dendrites. TLS-GFP clusters within spines were of a stationary nature. These data suggest that TLS may move dynamically within dendrites before spine maturation. However, once im-

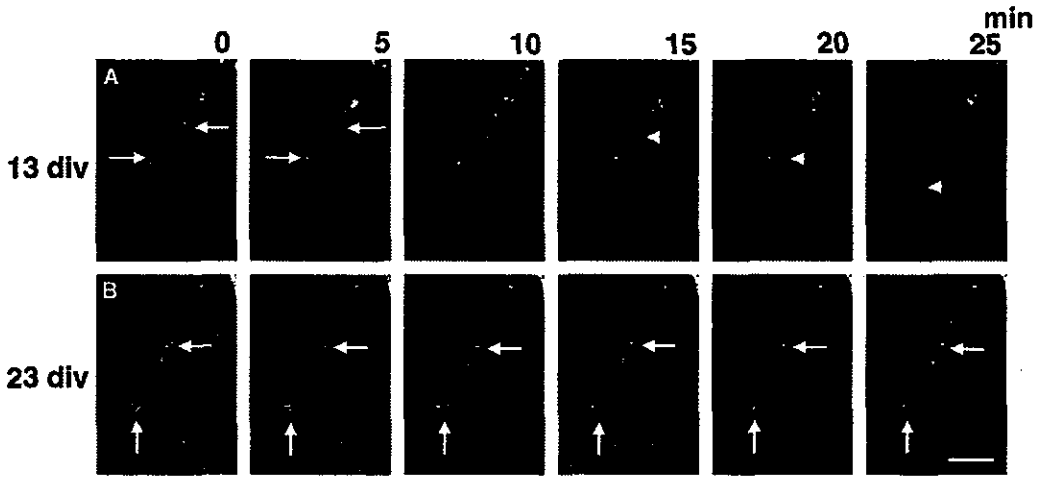

Figure 2. TLS-GFP Clusters Show Distinct Dynamics at Different Stages of Dendritic Maturation

TLS-GFP was expressed in mouse hippocampal neurons by use of the adenoviral expression system. TLS-GFP was assayed by time-lapse confocal imaging of TLS-GFP-expressing adenovirus 24–48 hr after the infection. (A) When TLS-GFP was expressed in immature dendrites with few spines (13 div: 13 days of in vitro culture), some TLS-GFP clusters fused together or dissociated during the short observation period of the time-lapse sequences (arrows in [A], 0–5 min). A fraction of TLS-GFP clusters actively moved a short distance in dendrites (arrowheads in [A], 15–25 min). (B) In mature dendrites (23 div: 23 days of in vitro culture), TLS-GFP clusters were stationary within spines and did not move as fast as they did in the immature dendrites. However, TLS-GFP clusters changed their shape actively, possibly because of the overall change of spine shape affected by actin-dependent motility (B, arrows). Scale bar, 5 μm.

mature spines are committed to form stable synapses, TLS may become preferentially recruited to and accumulated within spines.

Requirement of Intact Actin Polymers for TLS Translocation

To examine how the cytoskeletal organization of the dendrites is involved in the movement or transport of TLS, we treated primary cultured hippocampal neurons either with cytochalasin B or nocodazole, potent inhibitors of the assembly of actin filaments or microtubules, respectively. Both reagents affected the distribution of TLS within dendrites, and the TLS-GFP disappeared from the dendrites (Figure 1C). Quantitative analysis revealed a significant decrease in the TLS-GFP signal intensity in dendrites after treatment with either cytochalasin B or nocodazole (Figure 1C). On the other hand, the distribution of Staufen, whose dendritic localization is known to be microtubule dependent [12, 13], was affected by the nocodazole treatment, but not by cytochalasin B (Figure 1C). These data indicate that the dendritic localization of TLS-GFP required both actin filaments and microtubules.

Synaptic Activity-Dependent TLS Translocation to the Dendritic Spines

Mature dendrites expressing TLS-GFP were immunostained with anti-synapsin I antibody, anti-vesicular glutamate transporter-1 (VGLUT1) antibody, and anti-CortBP antibody to reveal the precise localization of TLS in dendrites. CortBP completely overlapped TLS-GFP at the synaptic sites (Figure S1F), whereas punctate structures immunopositive for either synapsin I, a marker of presynaptic vesicles, or VGLUT1, a marker of excitatory presynaptic structures, were closely apposed to the fluorescent clusters of TLS-GFP (Figure S1D and S1E, respectively), suggesting that TLS was specifically localized in the spines of excitatory postsynaptic sites, as described above.

Local protein synthesis subsequent to translocation of mRNA to dendrites is known to be stimulated by DHPG, a group 1 mGluR agonist [3], as well as neurotrophin, BDNF [14, 15]. Using DHPG to transiently activate mGluRs in dendrites, we tested to see if TLS-GFP accumulation in dendrites and dendritic spines depends on the state of synapse activation. When cultured hippocampal neurons expressing TLS-GFP were stimulated with DHPG (100 μM) over a 60-min period, the amount of TLS-GFP clusters in dendrites increased (Figures 3A–3D) and the movement of the particles accelerated (data not shown). Furthermore, the TLS-GFP clusters gradually accumulated in the dendritic spines (Figures 3A–3D, inset) where retrospective immunocytochemistry with synapsin I antibody revealed the presence of a presynaptic component at the sites of TLS accumulation (Figures 3D–3F). To the contrary, other synaptic proteins such as PSD95, Homer-1c (PSD-Zip45), Shank, and GKAP were not translocated into spines by DHPG treatment (see Figure S3). These results indicate that TLS is likely to be involved in the translocation of mRNA to the dendritic spines for local translation in dendrites. In DHPG-treated mature hippocampal neurons, the relative fluorescence intensity in spines was increased significantly (n = 26, cluster index 35% in average) by 5-fold compared with that of control neurons (n = 17, cluster index 7% in average) (Figure

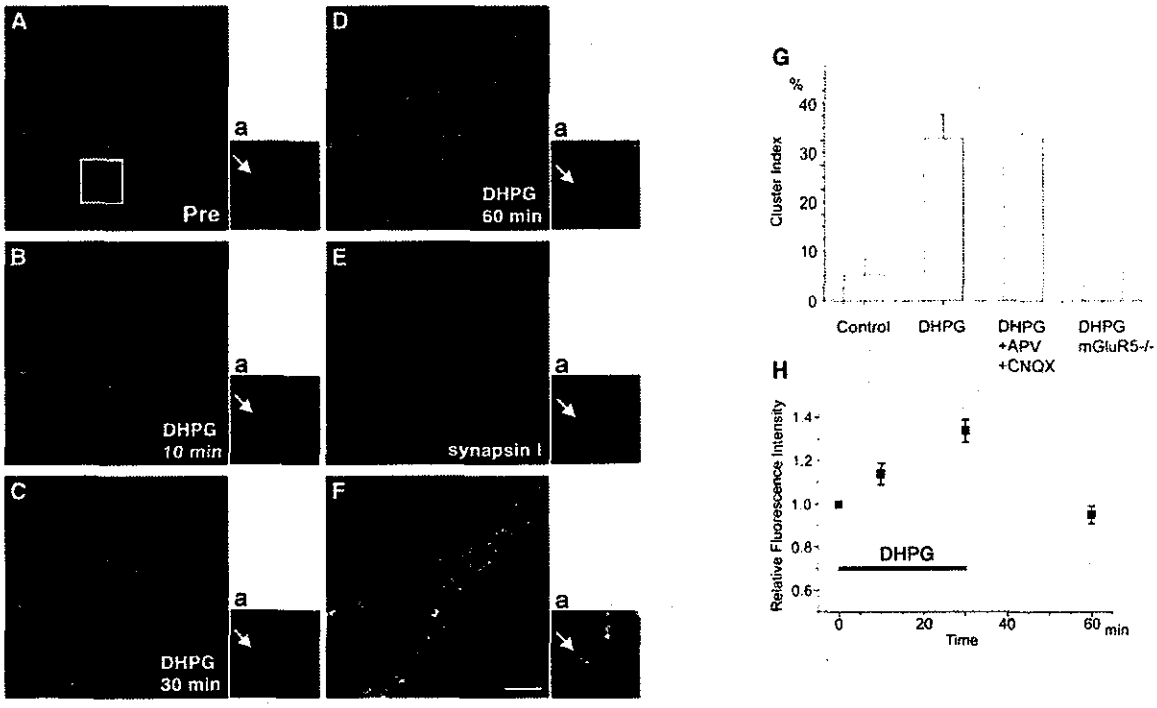

Figure 3. TLS Localization to the Postsynaptic Spines Is Dependent on mGluR Signals

(A–F) Time-lapse recording of TLS-GFP clusters after DHPG treatment (100 μM, 60 min) reveals that TLS-GFP accumulates within spines. (Aa–Fa) High-magnification view of the same area shown as a white rectangle in (A). Accumulation of TLS-GFP clusters takes place at the sites where retrospective immunocytochemistry by anti-synapsin I reveals the presence of presynaptic structures (E and F). Photos (F) and (Fa) are merged images of (D)–(E) and (Da)–(Ea), respectively.

(G and H) The average cluster index (the increase % of relative fluorescence intensity after the stimulation divided by the relative fluorescence intensity before the stimulation) is increased in cells treated with DHPG (n = 26). This DHPG-dependent effect does not change even in the combined presence of APV and CNQX (n = 7). The DHPG-dependent spine accumulation is abolished in hippocampal neurons from mGluR5$^{-/-}$ (n = 10). Control, n = 17 (H) DHPG (100 μM) induces accumulation of TLS-GFP in spines. However, upon the removal of DHPG 30 min after the start of treatment, the amount of TLS-GFP in spines returns to the control level. Error bars in (G) and (H) indicate SEM (n = 20).

3G). DHPG treatment did not change the number of the spines protruding from the shaft under the experimental conditions used nor caused significant elongation of the spines. Moreover, upon the removal of DHPG 30 min after the treatment, the number of spines containing TLS-GFP clusters moved back to the control level after another 30-min period of incubation (Figure 3H). This result clearly indicates that the spine localization induced by DHPG is a reversible event and that the spine localization was dependent on the state of mGluR activation. Hippocampal neurons expressing TLS-GFP were exposed to DHPG in the presence of both CNQX and APV, which are antagonists for the AMPA/kainate-type glutamate receptor (GluR) and NMDA receptor (NMDAR), respectively, to identify the signals responsible for the spine localization. The combination of CNQX and APV did not affect the DHPG-induced spine localization of TLS (Figure 3G), indicating that the spine localization was solely mediated by the mGluR activation and was independent of GluR or NMDAR activation. Because we demonstrated that TLS accumulated exclusively in the spines of postsynaptic neurons (Figure S1D–S1F), mGluR5, the major group 1 mGluR, was suspected to be the most plausible receptor candidate involved in TLS localization to the spines of pyramidal neurons in the CA1 area. To test this possibility, we examined the DHPG-induced TLS redistribution in hippocampal neurons derived from mGluR5 knockout mice [16]. In neurons of the mGluR5 homozygous mutants in which basal TLS distribution was not changed compared with wild-type (Figure S4), DHPG could not induce spine localization of TLS (Figure 3G). These results confirm that TLS accumulation in spines is induced upon postsynaptic activation of signaling cascades initiated by mGluR5.

Abnormal Spine Morphology in TLS-Deficient Mice

To investigate the context of TLS localization and its role in neuronal development, we prepared primary hippocampal neurons from embryos of TLS mutant mice (TLS$^{-/-}$) [17] and stained them with the lipophilic dye DiI (Figure 4). In the hippocampal neurons from the TLS-deficient mice, the dendrites were irregularly branched, and numerous long and thin processes like immature axons extended from the cell body (Figure 4A, arrows in upper panel of –/–), which is not observed in wild-type neurons extended with a single axon from the cell body (Figure 4A, arrows in upper panel of +/+). How-

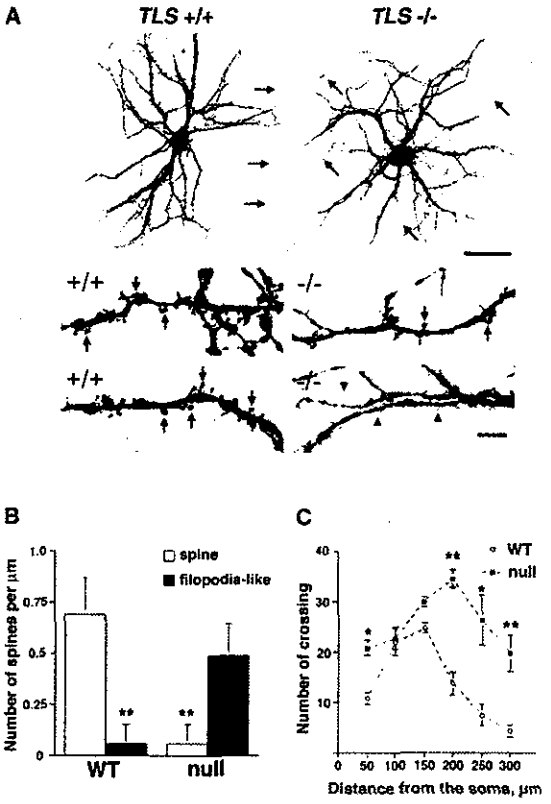

Figure 4. TLS-Deficient Mice Show Reduced Spine Number and Abnormal Spine Morphology

(A) Morphology of hippocampal neurons from TLS wild-type (*TLS*$^{+/+}$) and TLS null mutant (*TLS*$^{-/-}$) mice visualized by application of lipophilic dye DiI at 21 days in vitro. In neurons obtained from TLS$^{-/-}$ mice, there were multiple axon-like processes that have elongated from the soma (arrows in –/– of the upper panel). With higher magnification, the spines were reduced in their number (arrows in –/– of the middle panel) or transformed into thin cytoplasmic protrusion similar to filopodia (arrowheads in –/– of the lower panel). In contrast, majority of dendritic protrusions in wild-type neurons showed the morphology of mushroom-shaped spines, containing large heads connected to the shaft via thin neck (arrows in +/+ of the lower panels). Scale bars, 50 μm in upper panels and 5 μm in lower panels.

(B) Quantitative analysis of spine density in hippocampal neurons taken from wild-type (+/+) and TLS null mutant (–/–) mice. There was a significant decrease of spine density in the TLS null mice. On the other hand, the number of filopodia-like protrusions was significantly increased in TLS null neurons (50 representative dendrites from 10 neurons with each genotype were measured; double asterisk, $p < 0.01$). Error bars, SEM.

(C) Sholl profiles revealed a slight change in branching pattern of TLS null cultured pyramidal neurons. Number of dendritic crossings within 50 μm and over 200 μm from the soma significantly increased in TLS null neurons (n = 30 independent neurons). Asterisk, $p < 0.05$; double asterisk, $p < 0.01$.

ever, immunostaining for MAP2 or SMI31 revealed that TLS-null neurons possessed multiple dendrites and a single axon, indicating that the neuronal polarity was not affected by the TLS deficiency (data not shown). The spines in TLS-deficient neurons were reduced in number (Figure 4A, arrows in lower panel of –/–) or transformed into thin and long cytoplasmic protrusions similar to filopodia (Figure 4A, arrowheads in lower panel of –/–). Their structure was distinct from that of the wild-type hippocampal neuron spines, which displayed thin necks and relatively large heads and, thus, had a mushroom-like shape (Figure 4A, arrows in lower panel of +/+) [1]. Quantitative analysis revealed that the density of spines in TLS-deficient neurons was significantly reduced compared with that in the wild-type ones (Figure 4B). On one hand, the number of filopodia-like spines was increased in TLS-deficient neurons. To clarify further the difference in spine morphology between the TLS-deficient and wild-type neurons, we measured dendritic complexity by a standard Sholl analysis [18], which counts the number of dendritic crossings at 50 μm concentric circles. There were more branches in the proximal and distal region in TLS-deficient neurons compared with those in wild-type (Figure 4C). In the proximal region, more dendrites were elongated directly from the soma in the TLS null neurons. It appeared that there were more tertiary dendritic branches in the distal region of the TLS null neurons. These data imply a key role for TLS in neuronal maturation including dendritic branching and also maintenance of spine stability.

Discussion

Metabotropic glutamate receptors have diverse functions in signal transduction of neurons. Group 1 mGluRs, including mGluR1 and mGluR5, are localized at the periphery of the postsynaptic junctional membrane of principal neurons in the hippocampus and the cerebellum [19, 20]. Our time-lapse recording of TLS-GFP revealed that treatment with DHPG, a selective group 1 mGluR agonist, increased the amount of TLS-GFP clusters in the spines of mature dendrites within 30 min of stimulation (Figure 3). By using hippocampal neurons from mGluR5 knockout mice, we showed that postsynaptic mGluR5-mediated signaling system was responsible for the translocation of TLS. The reversal of TLS translocation after DHPG washout, shown in Figure 3H, clearly indicates that accumulation of TLS in spines was maintained by mGluR activity and not stabilized by other molecular interactions. Activated postsynaptic mGluR5 can induce increases in both intracellular calcium concentration $[Ca^{2+}]i$ and PKC activation through the G protein-linked inositol phospholipids pathway [21]. On the other hand, PKC activation has been shown to control the redistribution of a wide variety of proteins localized in the postsynaptic density (PSD) [22, 23]. Because PKC is responsible for the reorganization of the actin cytoskeleton in a variety of cell types [24], activation of PKC by mGluR5 may subsequently release TLS-containing RNA granules from their actin bound state and initiate their translocation into spines. This hypothesis can be tested by experiments with multiple fluorescent reporters to simultaneously monitor translocation of TLS and reorganization of the actin cytoskeleton.

Although DHPG treatment induces accumulation of TLS, signaling via mGluR5 cannot be the sole mechanism of TLS accumulation in spines. The presence of

another signaling system is evident from phenotypic examination of cultured neurons from mGluR5 null mice, where transition of TLS from dendritic shafts to spines took place with a time course similar to that for wild-type mice (unpublished data). On the other hand, absence of TLS in hippocampal neurons affected the morphology of the dendrites and reduced the number of the spines (Figure 4). It is likely that accumulation of TLS into spines is essential for their structural maturation but is dependent on multiple signaling systems including mGluR5 activation. Abnormal spine morphology has also been reported in FMRP null mice [25, 26]. In the FMRP knockout mice, neuronal dendrites exhibited long and thin dendritic spines with increased density. This increased spine density may be attributed to the absence of an activity-dependent translational suppression by FMRP [27]. The contrasting phenotypes of these null mutants illustrate the functional diversity of RNA binding proteins in dendrites.

Considering the dual functions of TLS as the RNA-splicing factor and an RNA transporter, we may speculate that TLS may coordinately regulate the rate of RNA splicing in the nucleus and the amount of mRNA transported to local translational machinery in spines in response to synaptic activation. Understanding how postsynaptic metabotropic signals regulate TLS dynamics will be essential in order to decipher the complex cellular system that integrates synaptic activity, RNA splicing and transport, and local dendritic translation. Our present and future findings on the neuronal functions of TLS do and will provide important keys for further understanding the molecular basis of synaptic plasticity and a general insight into local translation in polarized cells.

Supplemental Data

Supplemental Data include four figures, two movies, and Supplemental Experimental Procedures and are available with this article online at http://www.current-biology.com/cgi/content/full/15/6/587/DC1/.

Acknowledgments

We thank M. Kuno, T. Manabe, and H. Sabe for their helpful discussions. We greatly thank D. Ron and E. Schuman for the human TLS and the rat Staufen cDNA clones, respectively. We appreciate T. Ebihara and K. Sobue for kindly providing us CortBP antibody and J. Roder for the generous contribution of mGluR5-null mice. Finally, we thank Y. Sakakida and Y. Watanabe for mouse maintenance as well as K. Hamajima, I. Kawabata, and N. Takashima for their help with preparing the primary cultures of neurons. This work was supported in part by grants from the Ministry of Education, Culture, Sports, Science and Technology, Mitsubishi Pharma Research Foundation, Senri Life Science Foundation, and Sony Corporation. G.G.H. was supported by grants from the National Cancer Institute of Canada.

Received: September 1, 2004
Revised: January 5, 2005
Accepted: January 5, 2005
Published: March 29, 2005

References

1. Hering, H., and Sheng, M. (2001). Dendritic spines: structure, dynamics and regulation. Nat. Rev. Neurosci. *2*, 880–888.
2. Kiebler, M.A., and DesGroseillers, L. (2000). Molecular insights into mRNA transport and local translation in the mammalian nervous system. Neuron *25*, 19–28.
3. Job, C., and Eberwine, J. (2001). Localization and translation of mRNA in dendrites and axons. Nat. Rev. Neurosci. *2*, 889–898.
4. Steward, O., and Schuman, E.M. (2001). Protein synthesis at synaptic sites on dendrites. Annu. Rev. Neurosci. *24*, 299–325.
5. Steward, O., and Schuman, E.M. (2003). Compartmentalized synthesis and degradation of proteins in neurons. Neuron *40*, 347–359.
6. Crozat, A., Aman, P., Mandahl, N., and Ron, D. (1993). Fusion of CHOP to a novel RNA-binding protein in human myxoid liposarcoma. Nature *363*, 640–644.
7. Iko, Y., Kodama, T.S., Kasai, N., Oyama, T., Morita, E.H., Muto, T., Okumura, M., Fujii, R., Takumi, T., Tate, S., et al. (2004). Domain architectures and characterization of an RNA-binding protein, TLS. J. Biol. Chem. *279*, 44834–44840.
8. Zinszner, H., Sok, J., Immanuel, D., Yin, Y., and Ron, D. (1997). TLS (FUS) binds RNA in vivo and engages in nucleo-cytoplasmic shuttling. J. Cell Sci. *110*, 1741–1750.
9. de Hoog, C.L., Foster, L.J., and Mann, M. (2004). RNA and RNA binding proteins participate in early stages of cell spreading through spreading initiation centers. Cell *117*, 649–662.
10. Husi, H., Ward, M.A., Choudhary, J.S., Blackstock, W.P., and Grant, S.G. (2000). Proteomic analysis of NMDA receptor-adhesion protein signaling complexes. Nat. Neurosci. *3*, 661–669.
11. Kanai, Y., Dohmae, N., and Hirokawa, N. (2004). Kinesin transports RNA; isolation and characterization of an RNA-transporting granule. Neuron *43*, 513–525.
12. Kohrmann, M., Luo, M., Kaether, C., DesGroseillers, L., Dotti, C.G., and Kiebler, M.A. (1999). Microtubule-dependent recruitment of Staufen-green fluorescent protein into large RNA-containing granules and subsequent dendritic transport in living hippocampal neurons. Mol. Biol. Cell *10*, 2945–2953.
13. Tang, S.J., Meulemans, D., Vazquez, L., Colaco, N., and Schuman, E. (2001). A role for a rat homolog of staufen in the transport of RNA to neuronal dendrites. Neuron *32*, 463–475.
14. Kang, H., and Schuman, E.M. (1996). A requirement for local protein synthesis in neurotrophin-induced hippocampal synaptic plasticity. Science *273*, 1402–1406.
15. Schratt, G.M., Nigh, E.A., Chen, W.G., Hu, L., and Greenberg, M.E. (2004). BDNF regulates the translation of a select group of mRNAs by a mammalian target of rapamycin-phosphatidylinositol 3-kinase-dependent pathway during neuronal development. J. Neurosci. *24*, 7366–7377.
16. Lu, Y.M., Jia, Z., Janus, C., Henderson, J.T., Gerlai, R., Wojtowicz, J.M., and Roder, J.C. (1997). Mice lacking metabotropic glutamate receptor 5 show impaired learning and reduced CA1 long-term potentiation (LTP) but normal CA3 LTP. J. Neurosci. *17*, 5196–5205.
17. Hicks, G.G., Singh, N., Nashabi, A., Mai, S., Bozek, G., Klewes, L., Arapovic, D., White, E.K., Koury, M.J., Oltz, E.M., et al. (2000). Fus deficiency in mice results in defective B-lymphocyte development and activation, high levels of chromosomal instability and perinatal death. Nat. Genet. *24*, 175–179.
18. Sholl, D.A. (1953). Dendritic organization in the neurons of the visual and motor cortices of the cat. J. Anat. *87*, 387–406.
19. Baude, A., Nusser, Z., Roberts, J.D., Mulvihill, E., McIlhinney, R.A., and Somogyi, P. (1993). The metabotropic glutamate receptor (mGluR1 alpha) is concentrated at perisynaptic membrane of neuronal subpopulations as detected by immunogold reaction. Neuron *11*, 771–787.
20. Shigemoto, R., Nomura, S., Ohishi, H., Sugihara, H., Nakanishi, S., and Mizuno, N. (1993). Immunohistochemical localization of a metabotropic glutamate receptor, mGluR5, in the rat brain. Neurosci. Lett. *163*, 53–57.
21. Nakanishi, S. (1994). Metabotropic glutamate receptors: synaptic transmission, modulation, and plasticity. Neuron *13*, 1031–1037.
22. Fong, D.K., Rao, A., Crump, F.T., and Craig, A.M. (2002). Rapid synaptic remodeling by protein kinase C: reciprocal translocation of NMDA receptors and calcium/calmodulin-dependent kinase II. J. Neurosci. *22*, 2153–2164.
23. Lan, J.Y., Skeberdis, V.A., Jover, T., Grooms, S.Y., Lin, Y., Ar-

aneda, R.C., Zheng, X., Bennett, M.V., and Zukin, R.S. (2001). Protein kinase C modulates NMDA receptor trafficking and gating. Nat. Neurosci. *4*, 382–390.

24. Keenan, C., and Kelleher, D. (1998). Protein kinase C and the cytoskeleton. Cell. Signal. *10*, 225–232.
25. Comery, T.A., Harris, J.B., Willems, P.J., Oostra, B.A., Irwin, S.A., Weiler, I.J., and Greenough, W.T. (1997). Abnormal dendritic spines in fragile X knockout mice: maturation and pruning deficits. Proc. Natl. Acad. Sci. USA *94*, 5401–5404.
26. Nimchinsky, E.A., Oberlander, A.M., and Svoboda, K. (2001). Abnormal development of dendritic spines in FMR1 knock-out mice. J. Neurosci. *21*, 5139–5146.
27. Antar, L.N., and Bassell, G.J. (2003). Sunrise at the synapse: the FMRP mRNP shaping the synaptic interface. Neuron *37*, 555–558.

A Family-Based Association Study and Gene Expression Analyses of Netrin-G1 and -G2 Genes in Schizophrenia

Mika Aoki-Suzuki, Kazuo Yamada, Joanne Meerabux, Yoshimi Iwayama-Shigeno, Hisako Ohba, Kazuya Iwamoto, Hitomi Takao, Tomoko Toyota, Yumiko Suto, Noriaki Nakatani, Brian Dean, Sachiko Nishimura, Kenjiro Seki, Tadafumi Kato, Shigeyoshi Itohara, Toru Nishikawa, and Takeo Yoshikawa

Background: *The netrin-G1 (*NTNG1*) and -G2 (*NTNG2*) genes, recently cloned from mouse, play a role in the formation and/or maintenance of glutamatergic neural circuitry. Accumulating evidence strongly suggests that disturbances of neuronal development and the N-methyl-D-aspartate receptor–mediated signaling system might represent a potential pathophysiology in schizophrenia. We therefore set out to examine the genetic contribution of human* NTNG1 *and* NTNG2 *to schizophrenia.*

Methods: *Twenty-one single nucleotide polymorphisms (SNPs) from* NTNG1 *and 10 SNPs from* NTNG2 *were analyzed in 124 schizophrenic pedigrees. All genotypes were determined with the TaqMan assay. The expression levels of* NTNG1 *and* NTNG2 *were examined in the frontal (Brodmann's Area [BA]11 and BA46) and temporal (BA22) cortices from schizophrenic and control postmortem brains. The isoform-specific expression of* NTNG1 *splice variants was assessed in these samples.*

Results: *Specific haplotypes encompassing alternatively spliced exons of* NTNG1 *were associated with schizophrenia, and concordantly, messenger ribonucleic acid isoform expression was significantly different between schizophrenic and control brains. An association between* NTNG2 *and schizophrenia was also observed with SNPs and haplotypes that clustered in the 5′ region of the gene.*

Conclusions: *The* NTNG1 *and* NTNG2 *genes might be relevant to the pathophysiology of schizophrenia.*

Key Words: Neurodevelopment, laminet-1, laminet-2, postmortem brain, real-time quantitative polymerase chain reaction, alternative splicing

Schizophrenia is a severe brain disorder that usually produces a lifetime of disability, with emotional and cognitive distress for the affected individuals (Lewis and Lieberman 2000). Although schizophrenia has a worldwide prevalence of approximately 1%, the specific factors that underlie its predisposition remain elusive. A number of studies have focused on identifying genetic and environmental components that separately, or in combination, contribute to the manifestation of the disease (Lewis and Levitt 2002).

A strongly supported theory is that schizophrenia evolves from a fixed brain lesion occurring early in neurodevelopment that responds abnormally to later maturational stimuli (Chua and Murray 1996; Marenco and Weinberger 2000; Weinberger 1987). Developmental neurobiology has made great strides in detailing the molecular machinery that leads to the assembly of brain systems (Jessell 2000; Tessier-Lavigne and Goodman 1996). Several gene families that are responsible for encoding cues for guiding axonal growth cones and cell migration have been identified. These genes include members of the immunoglobulin superfamily, ephrins, semaphorins, slits, and netrins (Chisholm and Tessier-Lavigne 1999; Tessier-Lavigne and Goodman 1996). For the cellular and signaling bases for schizophrenia pathophysiology, disturbances in *N*-methyl-D-aspartate (NMDA) and dopamine neurotransmission have also been strongly implicated.

The netrins are a family of diffusible axon guidance molecules related to laminin that are conserved from *Caenorhabditis elegans* to vertebrates (Ishii et al 1992; Serafini et al 1994). A netrin-related molecule, netrin-G1 (Ntng1) (also called laminet-1), has been identified in mice and shown to be distinct from the classical netrins in several aspects (Nakashiba et al 2000; Yin et al 2002). Unlike classical netrins, Ntng1 is predominantly tethered to the membrane through a carboxyl-terminal glycosyl phosphatidyl-inositol anchor. It generates several splice variants, none of which bind deleted in colorectal carcinoma (DCC) or uncoordinated 5 (UNC5), the best characterized netrin receptors. Nakashiba et al (2002) and Yin et al (2002) have recently identified a close paralogue, netrin-G2 (Ntng2) (also called laminet-2). Both *Ntng1* and *Ntng2* are elaborated within the vertebrate lineage. Comparative analysis of mouse *Ntng1* and *Ntng2* revealed complementary expression in the brain, implying nonredundant roles (Nakashiba et al 2002; Yin et al 2002). Our ongoing studies with mutant mice devoid of these proteins suggest that Ntng1 and Ntng2 are necessary in correct NMDA receptor functioning and that mutant mice show behavioral phenotypes related to schizophrenia (Nishimura et al 2004).

To define the possible roles of *NTNG1* and *NTNG2* molecules in schizophrenia, we mapped the genomic layout of human *NTNG1* and *NTNG2*, confirmed their chromosomal localization, and detected multiple splice variants of *NTNG1* transcripts. On the basis of these findings, we performed a

From the Laboratories for Molecular Psychiatry (MAS, KY, JM, YIS, HO, HT, TT, NN, TY), Molecular Dynamics of Mental Disorders (KI, TK), and Behavioral Genetics (SN, KS, SI), RIKEN Brain Science Institute, Wako; Section of Psychiatry and Behavioral Sciences (MAS, TN), Tokyo Medical and Dental University Graduate School, Tokyo; Department of Pediatric Cardiology (YS), Tokyo Women's Medical University, Tokyo, Japan; and The Rebecca L. Cooper Research Laboratories (BD), Mental Health Research Institute of Victoria, Parkville, Victoria, Australia.

Address reprint requests to Takeo Yoshikawa, M.D., Ph.D., RIKEN Brain Science Institute, Laboratory for Molecular Psychiatry, 2-1 Hirosawa, Wako-city, Saitama 351-0198, Japan; E-mail: takeo@brain.riken.go.jp.

Received April 21, 2004; revised November 4, 2004; accepted November 11, 2004.

0006-3223/05/$30.00
doi:10.1016/j.biopsych.2004.11.022

genetic and expression study of these two closely related genes in schizophrenia.

Methods and Materials

Subjects

The schizophrenia pedigrees were all derived from a geographic area located in central Japan. The probands, both in- and outpatients, were followed up by hospital doctors for at least 6 months. The samples consisted of 124 families with 376 members, of whom 163 were affected. This included 1) 80 independent and complete trios (schizophrenic offspring and their parents); 2) 15 probands with one parent; 3) 13 probands with affected siblings; and 4) 30 probands with discordant siblings (Yamada et al 2004). There was some overlap in the samples from 1), 3), and 4). Consensual diagnosis was made according to DSM-IV criteria by at least two experienced psychiatrists, on the basis of direct interviews, available medical records, and information from hospital staff and relatives. None of the patients had additional Axis I disorders as defined by DSM-IV, and none of the present family members suffered from neurodegenerative disorders, including Parkinson's and Alzheimer's diseases.

The present study was approved by the ethics committee of RIKEN Brain Science Institute. All patients and family members gave informed and written consent to participate in the study.

Determination of the Exon/Intron Structures of NTNG1 and NTNG2

The complete genomic structure of *NTNG1* was not available from the databases and was determined as described (Meerabux et al, unpublished data): briefly, mouse netrin-G1a complementary deoxyribonucleic acid (cDNA) sequence NM_030699 and G1d sequence AB038664, as well as human *NTNG1* clones BC030220 and AB023193, were aligned with human genomic bacterial artificial chromosome (BAC) clones RP11-270C12, RP11-396N10, and RP11-436H6 (GenBank identification [ID] numbers AC114491, AL590427, and AL513187, respectively; http://www.ncbi.nlm.nih.gov/Entrez/index.html) using the National Center for Biotechnology Information (NCBI) BLAST 2 sequences algorithm (http://www.ncbi.nlm.nih.gov/blast/bl2seq/bl2.html). For *NTNG2* genomic organization, we consulted the Ensembl Human Genome Browser (http://www.ensembl.org/Homo_sapiens/), which provided annotation on the longest cDNA clone available in the databases (Vega Gene ID: OTTHUMG00000020835).

Fluorescent In Situ Hybridization (FISH)

For fluorescent in situ hybridization (FISH) analysis, *NTNG1* cDNA probe was prepared by polymerase chain reaction (PCR) amplification of Marathon-Ready Human adult brain cDNA (Clontech, Palo Alto, California) with a forward primer (5′-AGGGGGCGACTTGCAGGAGGC, 3′ end at nucleotide (nt) -570: A of the ATG initiation codon is counted as +1) and a reverse primer (5′-GCAGTGCCTTTGGGGATGGGG, 3′ end at nt 1032 in BC030220). The procedure was repeated for *NTNG2* (forward primer: 5′-CTGAGAGGTTCTGCTCCCATG, 3′ end at nt 3; reverse primer: GGGTAGCAGCCCTGGCGCCAG, 3′ end at nt 1313 in AB058760). The PCR products were separated on an agarose gel, and the DNA was excised, purified, and sequenced to check the fidelity of the probes. The purified DNA samples were fluorescently labeled under standard conditions and used as probes against normal metaphase chromosomes.

Detection of Ntng1 Transcript Isoforms

On the basis of information regarding the mouse *Ntng1* splice variation, which is generated by alternative splicing of downstream exons (Nakashiba et al 2000), we designed a PCR assay to detect human splice variants from Marathon-Ready Human adult brain cDNA (Clontech), using a forward primer designed to exon 4 and a reverse primer in exon 10 (Meerabux et al, unpublished data). The PCR products were cloned into pCR2.1 (Invitrogen, Carlsbad, California) and sequenced with the DYEnamic ET terminator cycle sequencing kit (Amersham Pharmacia Biotech, Piscataway, New Jersey). The exonic composition of each fragment was determined by aligning each sequence result against the known *NTNG1* exon sequences with SEQUENCHER software (Gene Codes, Ann Arbor, Michigan).

We also performed semiquantitative analysis of *NTNG1* messenger ribonucleic acid (mRNA) splice variants by separating the PCR fragments with an Agilent 2100 bioanalyzer with the DNA1000 LabChip kit (Agilent Technologies, Palo Alto, California). The bioanalyzer software automatically calculates migration time (sec), area, size (bp), concentration (ng/μL), and molarity (nmol/L) of each separated band and displays the results in real time. The identities of the detected peaks were determined by comparison with the cloned isoforms run in a separate well on the same chip.

Mutation Screening

Genomic DNA was isolated from blood samples according to standard methods. The complete coding region and exon/intron boundaries of *NTNG1* and *NTNG2* were screened for polymorphisms by direct sequencing of PCR products, from 40 unrelated schizophrenia samples. Primers used for amplification are listed in Appendix 1 (available online). Polymerase chain reaction was performed with an initial denaturation at 94°C for 1 min, followed by 35 cycles at 94°C for 15 sec, 50°–70°C (optimized for each primer pair) for 15 sec, 72°C for 45 sec, and a final extension at 72°C for 2 min, with TaKaRa Taq polymerase (Takara Bio, Shiga, Japan). Detailed information on amplification conditions is available upon request. Direct sequencing of PCR products was performed with the BigDye Terminator Cycle Sequencing FS Ready Reaction kit (Applied Biosystems, Foster City, California) and the ABI PRISM 3700 Genetic Analyzer (Applied Biosystems). Polymorphisms were detected with SEQUENCHER. The Japanese Single Nucleotide Polymorphisms (http://snp.ims.u-tokyo.ac.jp/index.html), The SNP Consortium (http://snp.cshl.org/news/), and the NCBI (http://www.ncbi.nlm.nih.gov/) databases were searched for additional single nucleotide polymorphisms (SNPs).

SNP Genotyping

Single nucleotide polymorphisms were typed in all 124 families with the TaqMan system (Applied Biosystems). Polymerase chain reactions were performed in an ABI 9700 thermocycler, and fluorescence was determined with an ABI 7900 sequence detector single point measurement and SDS v2.2 software (Applied Biosystems). Each marker was checked for allele–inheritance inconsistency within a pedigree with PEDCHECK software (O'Connell and Weeks 1998), and conflicts or flagged alleles were resolved by regenotyping.

Statistical Analyses

The initial panel of 124 families was analyzed with the pedigree disequilibrium test (PDT) program, v3.12 (http://www.chg.duke.edu/software/pdt.html) (Martin et al 2000, 2001). The statistically more conservative follow-up study was carried out

Table 1. Demographic and Treatment Data for the Australian Schizophrenic and Control Brains (BA11 and BA22)

Subject ID	Age (y)	Gender	PMI (h)	pH	Cause of Death	FRAD	FAPDD
Schizophrenic Patients							
1	79	F	26	6.27	Hypothermia	Fluphenazine decanoate	89
2	57	M	24	6.06	Coronary artery atheroma	Fluphenazine decanoate	45
3	65	M	41	6.57	Ischemic heart disease	Fluphenazine decanoate	45
4	47	F	50	6.31	Pneumonia	Resperidone	1200
5	65	F	50	6.35	Rupture of abdominal aortic aneurysm	Fluphenazine decanoate + haloperidol	339
6	69	M	48	6.44	Suicide: Carbon monoxide poisoning	Haloperidol	350
Mean ± SD	63.67 ± 10.86		39.83 ± 11.97	6.33 ± .17			
Control Subjects							
1	77	F	17	6.32	Hypertension heart disease		
2	57	M	27	6.43	Ischemic heart disease		
3	68	M	41	6.06	Aortic stenosis		
4	39	F	65	6.38	Mitral valve prolapse		
5	62	F	40	6.45	Ischemic heart disease		
6	68	M	69	6.59	Coronary artery atheroma		
Mean ± SD	61.83 ± 13.04		43.17 ± 20.52	6.37 ± .18			

BA, Brodmann's Area; ID, identification number; PMI, postmortem interval; FRAD, final recorded antipsychotic drug; FAPDD, final recorded antipsychotic drug dose (mg chlorpromazine equivalents/day); M, male; F, female.

with the complete 80-trio set and the extended transmission disequilibrium test (ETDT) algorithm, v2.2 (Sham and Curtis 1995). Empirical significance levels of the ETDT results were simulated from 10,000 Monte Carlo permutations with the MCETDT program, v1.3 (http://www.mds.qmw.ac.uk/statgen/dcurtis/software.html) (Zhao et al 1999). The TRANSMIT program, v2.5.4 (Clayton 1999; Clayton and Jones 1999) was used for haplotype-based transmission disequilibrium testing. Uncorrected p values for individual haplotypes (haplotypic p) and corrected p values for multi-allele testing (global p) were calculated with the TRANSMIT program.

Genomic linkage disequilibrium (LD) patterns retained in the Japanese population were determined by pairwise LD examination of markers within *NTNG1* and *NTNG2*, in 186 unrelated individuals from our schizophrenic pedigree panel. The standardized disequilibrium coefficient (D') (Lewontin 1988) and the squared correlation coefficient (r^2) were calculated with COCAPHASE software (http://www.hgmp.mrc.ac.uk/~fdudbrid/software/unphased/) (Dudbridge 2003).

Collection of Human Central Nervous System Tissues

Two sources of postmortem brain samples were used in this study. In one sampling, Brodmann's Area (BA)11 (lateral orbitofrontal cortex) and BA22 (superior temporal cortex) were collected by the Victorian Institute of Forensic Medicine, affiliated with the State Coroner's Office in Australia. At autopsy, brains were removed, and 1-cm coronal slices from the left hemispheres were rapidly frozen to −80°C. The postmortem diagnoses were confirmed according to DSM-IV criteria by a psychiatrist and a senior psychologist using the Diagnostic Instrument for Brain Studies (Keks et al 1999). Ethical approval for the study was given by the North-Western Healthcare Network Human Ethics Committee. The gender distribution, mean age, mean postmortem interval, and pH for the tissues were not significantly different between schizophrenia (n = 6) and control (n = 6) groups (Table 1). The control subjects had no known history of psychiatric illness.

The second set of samples consisted of RNA extracted from BA46 (dorsolateral prefrontal cortex [DLPFC]), obtained from the Stanley Foundation brain collection. Detailed information on the subjects and the extraction method are described on the web site, http://www.stanleyresearch.org/programs/brain_collection.asp. Both schizophrenia and control groups consisted of 27 subjects. Diagnoses were made according to DSM-IV. A summary of the demographic information on these subjects is shown in Table 2. There were no significant demographic differences between schizophrenic and control brains (Torrey et al 2000). This study was performed unblinded.

RNA Preparation and cDNA Synthesis

Total RNA was extracted from the brain sample with an acid guanidium thiocyanate/phenol chloroform extraction method (ISOGEN; NIPPON Gene, Toyama, Japan). In the Australian samples, single-stranded cDNA was synthesized with SuperScript III RT (Invitrogen, Carlsbad, California) and oligo(dT) and random hexamers. For the Stanley Foundation brain collection samples, the extracted RNA was purified by RNAeasy column (Qiagen, Hilden, Germany). Single-stranded cDNA was synthesized by SuperScript II RT (Invitrogen) and oligo(dT) primers (Invitrogen) and converted to double-stranded cDNA by T4 DNA polymerase (Invitrogen).

Real-Time Quantitative PCR

The mRNA levels were determined by real-time quantitative PCR, with TaqMan universal PCR mastermix, transcript-specific minor groove binding (MGB) probes (Assays-on-Demand, Applied Biosystems), and an ABI 7900 sequence detection system, according to the manufacturer's instructions. The MGB probe for total *NTNG1* (detects all isoforms) was derived from exons 3 and 4 and that for *NTNG2* from exons 1 and 2. The probe specific to each *NTNG1* isoform is described in the corresponding sections.

The β2-microgloblin gene was chosen as a control from the TaqMan Human Endogenous Control Plate (Applied Biosystems) after evaluation of 11 available internal control probes. The PCR assay was performed simultaneously with test and standard samples and no template controls in the same plate. A standard curve plotting the cycle of threshold values against input quantity (log scale) was constructed for both the β2-microgloblin gene

Table 2. Demographic and Treatment Data for the Stanley Schizophrenic and Control Brains (BA46)

Sample ID	Age (y)	Gender	PMI (h)	pH	Cause of Death	Lifetime Antipsychotics[a]	Sample ID	Age (y)	Sex	PMI (h)	pH	Cause of Death
Schizophrenic Patients (n = 27)							Control Subjects (n = 27)					
S1	45	F	52	8.51	Sucide: jumped	20,000	C1	49	M	48	8.5	Cardiac disease
S2	40	M	34	6.18	Pneumonia	75,000	C2	53	M	9	6.4	Cardiac disease
S3	51	M	43	6.63	Cardiac disease	130,000	C3	37	M	13	6.5	Cardiac disease
S4	19	M	28	6.73	Overdose	2,500	C4	51	M	31	6.7	Cardiac disease
S5	53	F	13	8.49	Cardiac disease	15,000	C5	53	M	28	6	Cardiac disease
S6	37	M	30	6.8	Cardiac disease	20,000	C6	38	F	33	6	Cardiac disease
S7	52	M	10	8.1	Cardiac disease	100,000	C7	38	F	26	6.7	Cardiac disease
S8	24	M	15	8.2	Sucide: overdose	12,000	C8	60	M	47	6.6	Cardiac disease
S9	39	M	80	6.6	Motor vehicle accident	120,000	C9	35	M	62	6.7	Myocarditis
S10	33	M	29	6.5	Cardiac disease	20,000	C10	34	M	22	6.48	Cardiac disease
S11	50	M	9	6.2	Cardiac disease	34,000	C11	45	M	29	6.94	Cardiac disease
S12	43	M	18	6.3	Cirrhosia	90,000	C12	34	F	24	6.67	Cardiac disease
S13	32	F	38	6.6	Sucide: jumped	10,000	C13	42	M	37	6.91	Cardiac disease
S14	35	M	47	6.4	Cardiac disease	200,000	C14	44	F	10	6.2	Cardiac disease
S15	44	M	32	6.67	Cardiac disease	20,000	C15	57	M	26	6.4	Cancer
S16	47	M	13	6.3	Acute pancreatitis	300,000	C16	45	M	18	8.81	Cardiac disease
S17	45	M	35	6.66	Cardiac disease	50	C17	49	M	23	6.93	Cardiac disease
S18	36	F	27	8.49	Sucide: hanging	600	C18	49	F	45	6.72	Cardiac disease
S19	53	M	38	8.17	Cardiac disease	120,000	C19	33	F	29	6.52	Asthama
S20	54	F	42	6.65	Pneumonia	400,000	C20	48	M	31	6.60	Cardiac disease
S21	44	F	26	8.58	Pulmonary thrombosis	50,000	C21	50	M	49	6.75	Cardiac disease
S22	39	M	28	6.6	Sucide: hanging	48,000	C22	32	M	13	8.57	Cardiac disease
S23	38	M	35	6.68	Overdose	15,000	C23	47	M	11	8.8	Cardiac disease
S24	43	M	65	6.67	Sucide: hanging	70,000	C24	48	M	31	6.67	Cardiac disease
S25	42	M	19	6.48	Cardiac disease	18,000	C25	48	M	24	6.91	Cardiac disease
S26	46	M	30	6.72	Pneumonia	200,000	C26	39	F	58	8.48	Cardiac disease
S27	59	F	38	6.93	Cardiac disease	30,000	C27	47	M	38	8.57	Cardiac disease
Mean ±	42.3 ±		32.1 ±	8.53 ±		78,524 ±		44.8 ±		29.7 ±	8.81 ±	
SD	9.1		16.3	.23		97,532		7.6		13.3	.28	

BA, Brodmann's Area; PMI, postmortem interval; F, female; M, male.
[a]Lifetime neuroteptic dose in fluphenazine milligram equivalent dose.

and the target molecules (*NTNG1* and *NTNG2*) for each PCR assay. All real-time quantitative PCR data was captured with SDS v2.2 (Applied Biosystems). The ratio of the relative concentration of the target molecule to β2-microglobulin gene (target molecule/β2-microglobulin gene) was calculated. We used the Mann-Whitney *U* test (two-tailed) to detect significant changes in gene expression levels for each gene.

Results

Genomic Organizations and Chromosomal Localizations of NTNG1 and NTNG2

The FISH analysis showed that human *NTNG1* and *NTNG2* map to chromosomes 1p13.3 and 9q34, respectively (Figure 1), in keeping with their database assignment, although the *NTNG2* probe showed weak signal at 12q24.3 in 20% of the cells. Genomic analysis demonstrated that the *NTNG1* spans 341 kilobases (kb) and is composed of 10 exons (Figure 2), whereas human *NTNG2* is encoded by eight exons and spans an interval of 82 kb (Figure 3). Both genes are located in schizophrenia linkage regions (Lewis et al 2003; Kaufman et al 1998).

Isoform Variation of NTNG1 Transcripts

Detection of human *NTNG1* mRNA is generally limited to brain and kidney by Northern analysis (Lin et al 2003). An initial assay of *NTNG1* splice products in human adult brain detected at least nine alternatively spliced transcripts, involving exons 5, 6, 7, 8, and 9 (Figure 4). The relative abundance of each isoform in postmortem brain samples is shown in Figure 5A. The main isoforms in the brain were G1a, G1c, and G1d (Figure 5B).

SNP Identification and Genetic Analyses

Our mutation screening and database search detected a total of 21 SNPs in *NTNG1* (2 novel SNPs in our mutation screening) (Figure

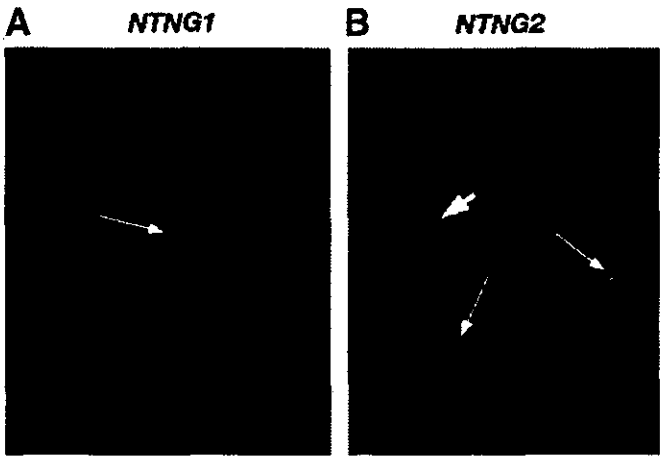

Figure 1. Fluorescence in situ hybridization of netrin-G1 **(A)** and netrin-G2 **(B)** sequences to normal metaphase human chromosomes. **(A)** The arrow denotes the positive signal at 1p13. **(B)** The thin arrows show the signal at 9q34, and the thick arrow shows weak signal at 12q24.

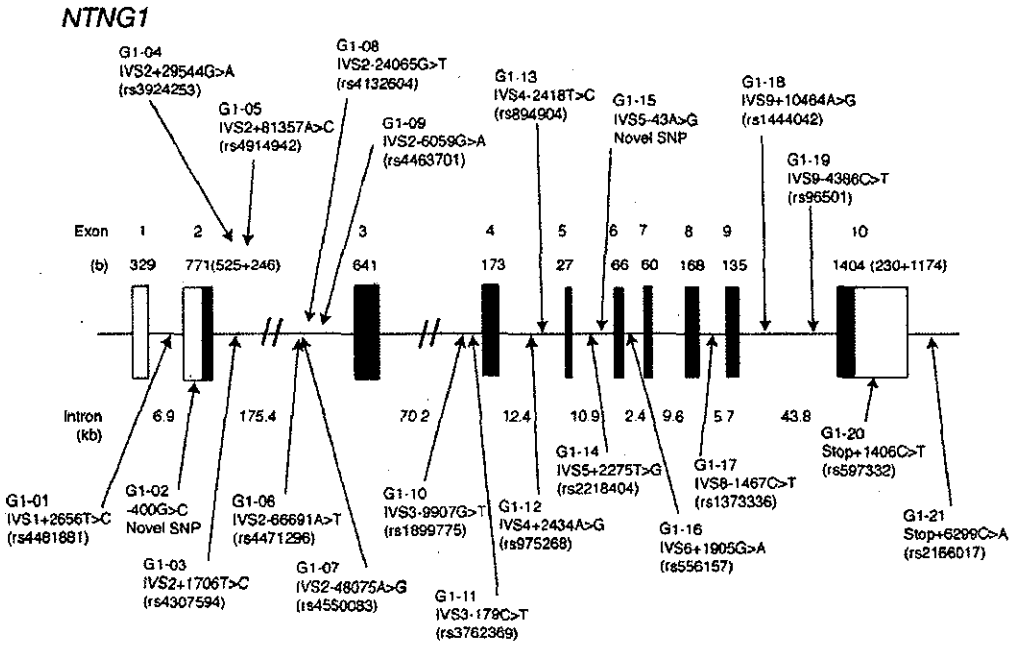

Figure 2. Genomic structure and location of polymorphic sites for human *NTNG1*. Exons are denoted by boxes, with untranslated regions in white and translated regions in black. The sizes of exons (bp) and introns (kb) are also shown. The rs number of each single nucleotide polymorphism (SNP) is the National Center for Biotechnology Information SNP cluster identification number from the dbSNP database (http://www.ncbi.nlm.nih.gov/SNP/).

2) and 10 SNPs in *NTNG2* (6 SNPs in our screening) (Figure 3). SNPs -400G>C (G1-02) and IVS5-43A>G (G1-15) in *NTNG1* and IVS4-15G>A (G2-09) in *NTNG2* were novel. No TaqMan typing probe could be designed for G2-09 in *NTNG2*. All other SNPs were unambiguously typed, with the exceptions of IVS4+2434A>G (G1-12) and Stop+1406C/T (G1-20) in *NTNG1*. The detailed information on these SNPs including heterozygosity is shown in Table 3. For subsequent genetic analyses, we chose 12 SNPs in *NTNG1* and 8 SNPs in *NTNG2*, on the basis of their relative abundance, with minor allele frequencies greater than .04 (Table 3).

Two different pairwise LD statistics, D' (normalized D) and r^2 (squared correlation coefficient) values, both of which measure LD values between 0 and 1, were computed between markers within the two genes, in 186 unrelated individuals from the present pedigree panel. Abecasis et al (2001) suggested a D' value greater than .33 as the minimum useful amount of LD, whereas Nakajima et al (2002) designated $r^2 > .1$ as the criterion for useful LD. In *NTNG1*, LD blocks with moderate strength exist in the intervals of G1-01 through to G1-03 and G1-11 through to G1-18 (Table 4). In *NTNG2*, intermediate LD measured by D',

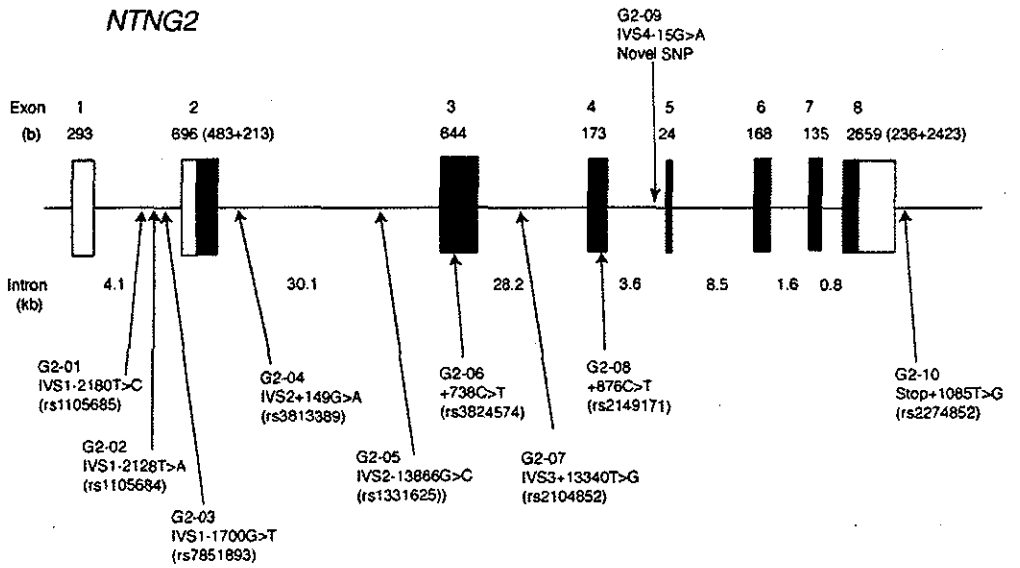

Figure 3. Genomic structure and locations of polymorphic sites for human *NTNG2*. Exons are denoted by boxes, with untranslated regions in white and translated regions in black. The sizes of exons (bp) and introns (kb) are also shown. The rs number of each single nucleotide polymorphism (SNP) is the National Center for Biotechnology Information SNP cluster identification number.

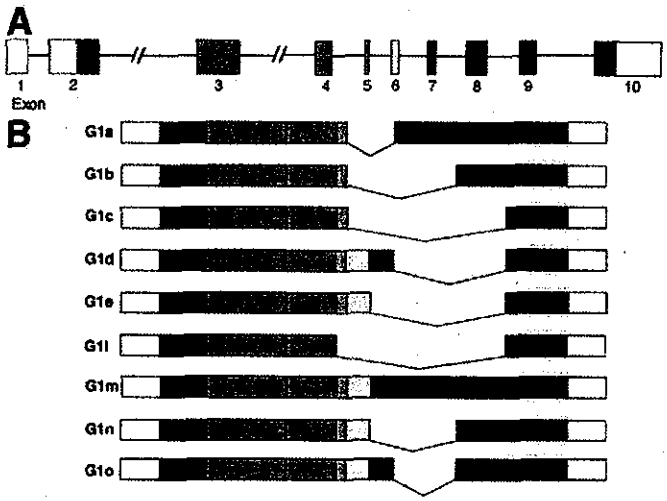

Figure 4. Splicing patterns of *NTNG1*. **(A)** All exons of *NTNG1*, with untranslated regions denoted in white and translated regions in color. **(B)** The nine different messenger ribonucleic acid isoforms.

was observed among the markers in the 5′ region of the gene (G2-01–G2-06) (Table 5).

Table 6 shows the results of family-based association tests for the entire pedigree panel. The PDT program computes two statistical measures, PDT-sum and PDT-ave. Briefly, PDT-sum gives more weight to larger families, whereas PDT-ave places equal weight on all families. The suitability of both statistical methods depends on family structure and genetic models (Martin et al 2001). In *NTNG1*, the SNP G1-19 showed significant association with schizophrenia (nominal $p = .02$) by PDT-sum. In *NTNG2*, the SNP G2-02 displayed significant association with schizophrenia with both PDT-sum ($p = .008$) and PDT-ave ($p = .014$). The SNPs G2-03 ($p = .022$) and G2-06 ($p = .045$) detected nominally significant associations by PDT-sum. After corrections for multiple SNP testing, the empirical p values for SNP transmission of *NTNG1* were .703 (PDT-ave) and .416 (PDT-sum), and those for *NTNG2* were .144 (PDT-ave) and .060 (PDT-sum). To test the SNP associations in a more stringent manner, we performed ETDT analysis on the 80 complete triad families. This detected a significant association between the G2-02 of *NTNG2* and schizophrenia ($p = .045$) (Table 6).

The transmission of individual haplotypes (haplotypic p) was assessed with the TRANSMIT program (Table 6). Significant distortions of haplotype transmission were observed for multiple haplotype blocks in *NTNG1* and *NTNG2* based on haplotypic p values, but the global p values were significant only with the (G1-14)–(G1-17)–(G1-18) haplotype of *NTNG1* ($p = .049$) and with the G2-02~G2-03 haplotype of *NTNG2* ($p = .049$). After Bonferroni correction for multiple testing, these transmission deviations were not significant. Further inspection of individual haplotypes revealed that the G-C-A haplotype (G1-14~G1-17~G1-18) of *NTNG1* was significantly less frequently transmitted ($p = .002$) and the A-T haplotype (G2-02~G2-03) of *NTNG2* was excessively transmitted ($p = .016$) to patients (Table 7), suggesting a protective role for the former and a risk factor for the latter.

Expression Analyses of NTNG1 and NTNG2 in Postmortem Brains

We quantified *NTNG1* and *NTNG2* mRNA expression levels in the two frontal regions BA11 (lateral orbitofrontal cortex) and BA46 (DLPFC) and one temporal region BA22 (superior temporal cortex) from schizophrenic and control postmortem brains, using MGB reactions. We analyzed six BA11 and six BA22 tissues each from schizophrenic patients and control subjects and 27 BA46 samples each from patients and control subjects. For *NTNG1*, transcript expressions were not significantly different between schizophrenic patients and control subjects in the three brain regions (Figure 6); nor were there significant differences in *NTNG2* expression levels between schizophrenic patients and normal subjects in the brain regions examined (Figure 6).

Expression Analysis of NTNG1 Isoforms

The *NTNG1* expression assay designed to detect the common exons 3 and 4 showed no significant changes between schizophrenic and control brains (Figure 6); however, because the haplotype spanning the alternatively spliced exons in *NTNG1* and composed of genetic variants (G1-14, G1-17, and G-18)

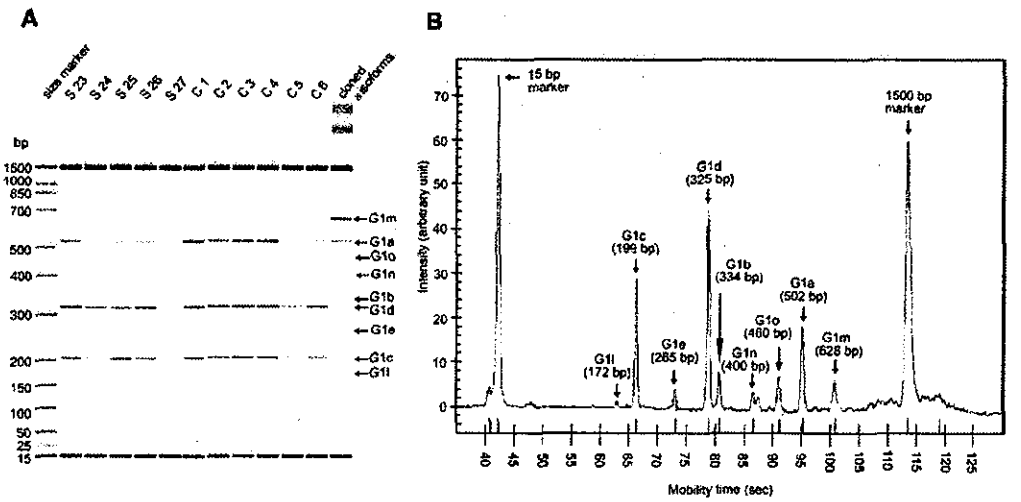

Figure 5. Demographic examples of semiquantitative analysis of *NTNG1* isoforms by the Agilent 2100 bioanalyzer using the DNA1000 LabChip kit. **(A)** Each analysis was represented by one lane in the gel-like image. The brain samples were Brodmann's Area 46 from the Stanley Foundation brain collection. Each sample number corresponds to the "Sample ID" shown in Table 2. The 15-bp and 1500-bp size markers were included in all samples for calibration of size and total amount. **(B)** The analysis of the S25 sample is presented as an electropherogram.

Table 3. Allele Frequencies for SNP Markers Located Within *NTNG1* and *NTNG2*

Marker No.	Polymorphism[a]	Genome Location by UCSC (bp)[b]	Distance from Neighboring SNP (bp)	Minor Allele Frequency[c]	Heterozygosity[c]
NTNG1		Chromosome 1p13.3			
G1-01	IVS1+2656T/C	107398460		.339	.448
G1-02	−400G/C	107402858	4398	.095	.171
G1-03	IVS2+1706T/C	107405209	2351	.289	.411
G1-04	IVS2+29544G/A	107433047	27838	.209	.330
G1-05	IVS2+81357A/C	107484861	51814	.048	.091
G1-06	IVS2−66691A/T	107512251	27390	0	0
G1-07	IVS2−48075A/G	107530867	18616	0	0
G1-08	IVS2−24065G/T	107554881	24014	.462	.497
G1-09	IVS2−6059G/A	107572887	18006	0	0
G1-10	IVS3−9907G/T	107639911	67024	0	0
G1-11	IVS3−179C/T	107649639	9728	.238	.363
G1-12	IVS4+2434A/G	107652424	2785	ND	
G1-13	IVS4−2418T/C	107659928	7504	.238	.363
G1-14	IVS5+2275T/G	107664647	4719	.238	.363
G1-15	IVS5−43A/G	107873201	8554	.035	.068
G1-16	IVS6+1905G/A	107675214	2013	.016	.032
G1-17	IVS8−1467C/T	107689862	14648	.347	.453
G1-18	IVS9+10464A/G	107701927	12085	.323	.437
G1-19	IVS9−4386C/T	107730889	28962	.194	.312
G1-20	Stop+1406C/T	107736910	6021	ND	
G1-21	Stop+6299C/A	107741803	4893	0	0
NTNG2		Chromosome 9q34			
G2-01	IVS1−2180T/C	132069110		.054	.102
G2-02	IVS1−2128T/A	132069162	52	.173	.286
G2-03	IVS−1700G/T	132069590	428	.284	.407
G2-04	IVS2+149G/A	132072134	2544	.071	.132
G2-05	IVS2−13866G/C	132089041	16907	.116	.205
G2-06	738C/T	132103431	14390	.390	.476
G2-07	IVS3+13340T/G	132116890	13459	0	0
G2-08	876C/T	132131808	14918	.465	.498
G2-09	IVS4−15G>A	132135498	3690	ND	
G2-10	Stop+1085T/G	132148138	12640	.446	.494

SNP, single nucleotide polymorphism; ND, genotypes were not unambiguously determined.
[a]Second allele is a minor allele.
[b]Data on May, 2004; UCSC: University of California, Santa Cruz.
[c]Based on the genotype data from *186 unrelated subjects.*

showed a preferential transmission to schizophrenic probands (global $p = .049$) (Table 6), we examined the composition of mRNA isoforms in BA46 of postmortem brains in a semiquantitative manner, using the Agilent bioanalyzer system (Figure 5A). Because semiquantitave analysis suggested differential expressions of the three main isoforms, G1a, G1c, and G1d, between schizophrenic and control brains (data not shown), we measured these transcripts in a more stringent manner, by design-

Table 4. Pairwise Marker-to-Marker LD Statistics of *NTNG1*

SNP Marker	G1-01	G1-02	G1-03	G1-04	G1-05	G1-08	G1-11	G1-13	G1-14	G1-17	G1-18	G1-19
G1-01		.939[a]	.887[a]	.386[a]	.180	.046	.052	.052	.052	.039	.200	.084
G1-02	.189[a]		1.000[a]	.069	.873[a]	.671[a]	.036	.036	.036	.214	.114	.013
G1-03	.628[a]	.260[a]		.150	.193	.231	.055	.055	.055	.104	.074	.153
G1-04	.020	.002	.002		.067	.670[a]	.006	.006	.008	.084	.020	.084
G1-05	.003	.004	.005	.001		1.000[a]	.144	.144	.144	.429[a]	.013	.217
G1-08	.001	.041	.019	.101	.042		.319[a]	.319[a]	.319[a]	.057	.238	.083
G1-11	.000	.000	.000	.000	.003	.027		1.000[a]	1.000[a]	1.000[a]	.901[a]	.143
G1-13	.000	.000	.000	.000	.003	.027	1.000[a]		1.000[a]	1.000[a]	.901[a]	.143
G1-14	.000	.000	.000	.000	.003	.027	1.000[a]	1.000[a]		1.000[a]	.901[a]	.143
G1-17	.001	.002	.008	.001	.005	.002	.166[a]	.166[a]	.166[a]		.960[a]	.253
G1-18	.010	.001	.001	.000	.000	.031	.120[a]	.120[a]	.120[a]	.233[a]		.148
G1-19	.001	.000	.002	.006	.010	.002	.002	.002	.002	.008	.011	

For each pair of markers, the standardized D' is shown above the diagonal, and r^2 is shown below the diagonal. LD, linkage disequilibrium; SNP, single nucleotide polymorphism.
[a]D' values of >.3 and r^2 values of >.1.

Table 5. Pairwise Marker-to-Marker LD Statistics of *NTNG2*

SNP Marker	G2-01	G2-02	G2-03	G2-04	G2-05	G2-06	G2-08	G2-09
G2-01		1.000[a]	1.000[a]	.025	1.000[a]	1.000[a]	.661[a]	.092
G2-02	.012		1.000[a]	1.000[a]	.049	.794[a]	.119	.154
G2-03	.146[a]	.506[a]		.787[a]	.448[a]	.443[a]	.116	.164
G2-04	.000	.017	.121[a]		.046	.416[a]	.280	.418[a]
G2-05	.008	.002	.010	.000		.643[a]	.080	.215
G2-06	.036	.199[a]	.122[a]	.020	.085		.136	.004
G2-08	.029	.003	.006	.005	.001	.014		.176
G2-10	.001	.004	.008	.011	.005	.000	.022	

For each pair of markers, the standardized D' is shown above the diagonal, and r^2 is shown below the diagonal. LD, linkage disequilibrium; SNP, single nucleotide polymorphism.

[a] D' values of >.3 and r^2 values of >.1.

Table 6. Transmission Analyses of Each SNP and Haplotype for *NTNG1* and *NTNG2* by PDT and ETDT

	PDT		ETDT	TRANSMIT							
Genes and Polymorphisms	SUM PDT	AVE PDT	Allele	Specific Haplotype p (2 SNPs)[a] Global p[c]				Specific haplotype p (3 SNPs)[b] Global p[c]			
NTNG1											
G1-01	.337	.168	.172	.162							
G1-02	.199	.156	.222	.371	.099			.177			
G1-03	.284	.247	.117		.216	.039[d]		.492	.061 .396		
G1-04	1.000	.509	.504			.177	.181			.026[d] .303	
G1-05	.695	1.000	.667	.124			.402				.095 .517
G1-08	.758	.992	.392	.256	.335			.207 .563			
G1-11	.833	.626	.891		.795	.809			.361 .809		
G1-13	.753	.542	1.000			.809	.809			.809 .809	
G1-14	.753	.542	1.000	.045[d]			.809				.045[d] .112
G1-17	.120	.172	.199	.112	.068			.002[a] .049[d]			
G1-18	.855	.647	.692		.289	.154			.094 .261		
G1-19	.020[d]	.088	.095			.284					
NTNG2											
G2-01	.655	.571	.761	.046[d]							
G2-02	.008[d]	.014[d]	.045[d]	.119	.018[d]			.016[d] .098			
G2-03	.022[d]	.061	.264		.049[d]	.062			.016[d] .057		
G2-04	.748	.571	1.000	.056		.090				.043[d] .098	
G2-05	.121	.118	.076	.143	.019[d]						.041[d] .068
G2-06	.045[d]	.055	.199		.088	.099		.035[d] .362			
G2-08	.421	.749	.535	.235		.373			.114 .707		
G2-10	.571	.724	.802	.664							

SNP, single nucleotide polymorphism; PDT, pedigree disequilibrium test; ETDT, extended transmission DT.

[a] For two-marker analysis, a sliding window of two markers was tested, with one-marker overlap.

[b] For three-marker analysis, a sliding window of three markers was tested, with two-marker overlap.

[c] The global p values represent the overall significance when the observed versus expected frequencies of all of the haplotypes are considered together.

[d] $p < .05$.

Table 7. *Transmission of Individual NTNG1 and NTNG2* Haplotypes that Showed Global Significance in Transmission Analyses

Gene and Haplotype	Observed Transmissions	Expected Transmissions	Var (O-E)	χ^2	*p* Value (1 df)
NTNG1 (G1-14)-(G1-17)-(G-18)					
G-C-A	7.0	15.3	7.0	9.741	.002[a]
T-C-A	36.0	35.0	13.0	.077	.781
G-T-A	63.0	56.7	18.3	2.145	.143
G-C-G	51.0	50.5	16.7	.016	.900
T-C-G	1.0	1.0	.5	.000	.989
G-T-G	2.0	1.5	.8	.325	.569
NTNG2 (G2-02)-(G2-03)					
T-G	107.0	111.9	15.9	1.518	.218
A-G	0	.5	.3	1.028	.311
T-T	18.0	20.6	6.8	.981	.322
A-T	35.0	27.0	11.0	5.817	.016[a]

[a] $p < .05$.

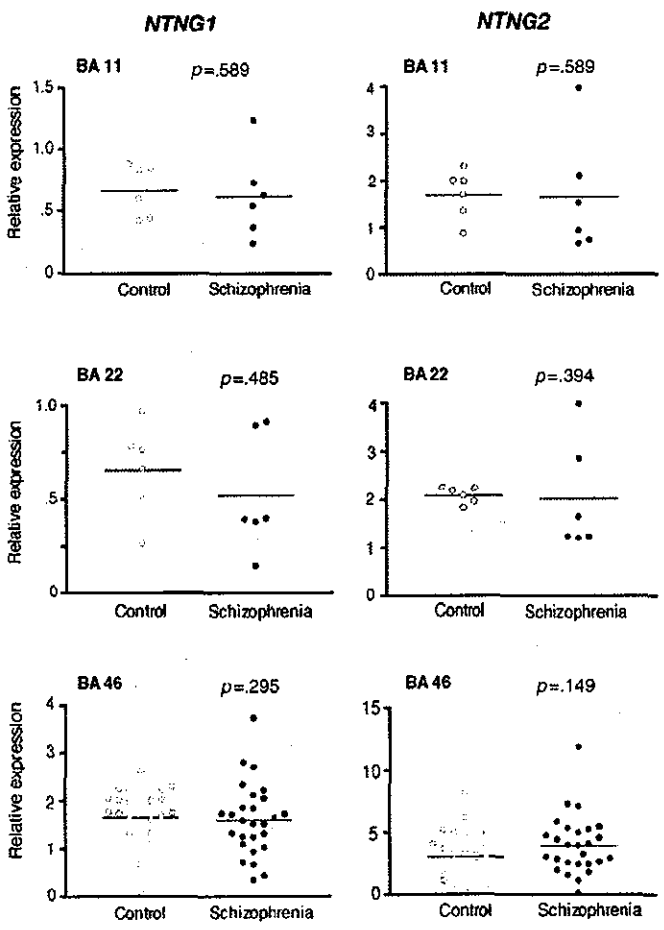

Figure 6. Messenger ribonucleic acid levels for *NTNG1* and *NTNG2* in the indicated brain regions (Brodmann's Area [BA]11, BA22, and BA46) of control and schizophrenic subjects. Each data point represents the relative expression level against that of the internal control (β2-microgloblin) for each sample. Horizontal bars indicate the mean value. BA11 and BA22 samples were from the Victorian Institute of Forensic Medicine in Australia ($n = 6$ for each group) and BA 46 were obtained from the Stanley Foundation brain collection ($n = 27$ for each group). The *p* values were calculated by Mann-Whitney *U* test (two-tailed).

ing isoform-specific PCR primers and TaqMan MGB probes (Figure 7). This quantitative analysis showed that the expression levels of G1c ($p = .013$) and G1d ($p = .015$) were significantly decreased in schizophrenic compared with control brains (Figure 7).

Discussion

In contrast to the classical netrin genes, netrin-G1 and -G2 are specific for vertebrates. In situ hybridization studies in mice show that *Ntng1* and *Ntng2* expression overlaps in limited brain areas (Nakashiba et al 2000, 2002). Mouse *Ntng1* is expressed with greatest abundance in the dorsal thalamic nuclei and the inferior colliculus, followed by perforant pathways of the entorhinal cortex and the olfactory pathway in the piriform cortex. Strikingly, mouse *Ntng2* expression occurs widely in the cerebral cortex and in the habenular nucleus and superior colliculus but not in regions that show *Ntng1* positivity. Northern analysis of human tissue also indicates that in the brain, *Ntng1* is expressed maximally in thalamic regions (Lin et al 2003). This spatial dissociation is suggestive of a specific role for each gene in these areas, and the strong expression in the thalamus and cortical areas hint that the role of netrin-Gs could include maintaining neuronal plasticity associated with sensory and/or cognitive functioning (Nakashiba et al 2002).

Abnormalities in measures of attention and cognition have been observed in patients with schizophrenia. These deficits might be linked to impairments in sensorimotor gating, whereby intrusive, overwhelming stimuli are improperly filtered (Braff and Geyer 1990). Interestingly, *Ntng1* knockout mice exhibit a reduced level of prepulse inhibition (Nishimura et al 2004), a behavioral paradigm that examines sensory filtering function (Geyer et al 2001). Furthermore, in the same study of mice lacking *Ntng1*, animals displayed an augmented behavioral sensitization to repeated administration of a noncompetitive NMDA receptor antagonist, dizocilpine (MK-801), and mice devoid of *Ntng1* or *Ntng2* showed reduced NMDA receptor–mediated postsynaptic responses in electrophysiologic analysis of brain slices (Nishimura et al 2004 and unpublished data). These data demonstrate that the proteins Ntng1 and Ntng2 are imperative for NMDA receptor function, lending further support to the disturbance of NMDA neurotransmission hypothesis for schizophrenia.

Our association analysis of the *NTNG1* gene detected a nominal association of the most 3′ variant G1-19 with schizophrenia. More importantly, the haplotype block constructed

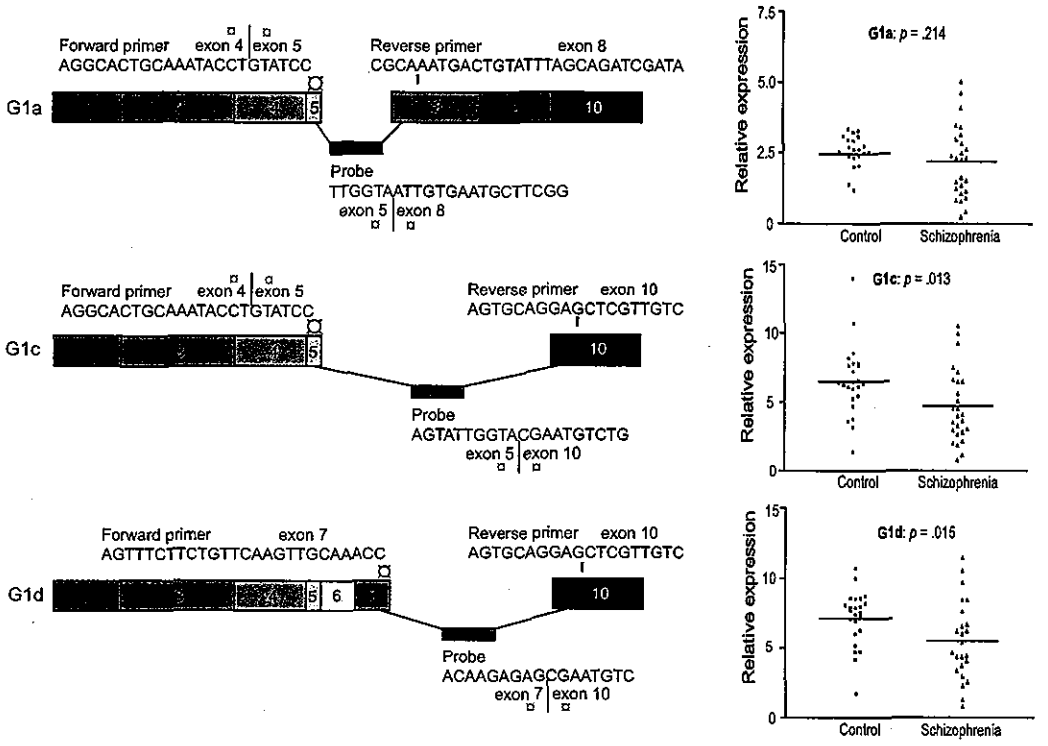

Figure 7. Isoform-specific expression analyses of *NTNG1*. **(A)** The design of polymerase chain reaction primers and TaqMan minor groove binding probes to analyze the three main isoforms G1a, G1c, and G1d. **(B)** Results of quantitative analysis of *NTNG1* isoforms. Each data point represents the relative expression level of a splice variant against that of the internal control (β2-microgloblin) for each brain sample. The data for failed amplifications are omitted. Horizontal bars indicate the mean value. The brain samples were Brodmann's Area 46 from the Stanley Foundation brain collection. The *p* values were calculated by the Mann-Whitney *U* test.

by G1-14~G1-17~G1-18, located in the 3′ region of the gene showed a globally significant excess of transmission to the disease. These results suggest that a potential disease-causing variant(s) might reside in the 3′ region of the gene. The mouse genomic structure of *Ntng1* is very similar to that of the human orthologue, as is the generation of multiple mRNA isoforms by alternative splicing (Nakashiba et al 2000). In humans, splicing involves the exons 5, 6, 7, 8, and 9. These exons are within the same LD block and overlap with the associated haplotype block. Therefore it is tempting to speculate that aberrant transcript processing might underpin this genetic association. In support of this speculation, splice variant netrin-G1c and -G1d distributions were significantly different between the DLPFC (BA46) of schizophrenic patients and control subjects. Although netrin-G1c and -G1d bind equally well to the NTNG1 ligand (NGL-1), the first molecule known to interact extracellularly with NTNG1 (Lin et al 2003; Nishimura et al, unpublished data), these isoforms might have distinct affinities for other unknown interacting molecules.

Both individual SNP and haplotype transmissions suggest a possible association between *NTNG2* and disease. The association signals were clustered within the same LD block located in the 5′ region of the gene. These results imply that the risk variant(s) might influence the regulation of gene expression. Our quantification assay, however, did not detect significantly different expression of *NTNG2* mRNA in BA46 of schizophrenic and control brains. A larger number of brain samples need to be examined before firm conclusions regarding differential gene expression between groups (schizophrenic vs. control) and regarding haplotype-dependent expressional levels of both *NTNG1* and *NTNG2* in each group can be drawn. Having stated this, it is practically and technically difficult to determine the exact haplotypes of genetically independent brain samples in the case of *NTNG1* (the SNPs G1-14, G1-17, and G1-18 of *NTNG1* span approximately 40 kb in the genome).

The anatomic significance of the frontal cortex in the pathogenesis of schizophrenia has long been recognized (Wong 2003). The DLPFC circuit involves the DLPFC in the cortex, the dorsolateral caudate nucleus of the striatum, the lateral dorsal medial nucleus of the globus pallidus, the posterolateral nucleus of the substantia nigra, and the ventral anterior, medial dorsalis, pars parvocellularis subnuclei of the dorsal medial nucleus of the thalamus. Defects in any of these structures could produce alterations in intrinsic and extrinsic functional connectivity that might be related to the symptomology of schizophrenia (Bunney et al 2000). In this context, the present findings of a potential disturbance of at least *NTNG1* gene regulation at the transcriptional level might suggest a molecular contribution by netrin-G gene(s) to the disrupted higher-order brain functions in schizophrenia.

In conclusion, our data suggest a possible involvement of human *NTNG1* and *NTNG2* in the vulnerability to schizophrenia; however, to draw a robust conclusion regarding the disease-promoting role of these vertebrate-specific genes, further replication studies are warranted in independent samples. In addition, it would be interesting to include the gene for transmembrane protein NGL-1, which has recently been identified as a specific binding partner of NTNG1 (Lin et al 2003), in future genetic studies to determine the role of the netrin-G system in schizophrenia.

This work was supported by RIKEN BSI Funds, the RIKEN President Fund, Research on Brain Science Funds from the Ministry of Health Labor and Welfare, and CREST funds from the Japan Science and Technology Agency, Japan.

This article is dedicated to Dr. Masayuki Fukasawa (1973–2004).

Abecasis GR, Noguchi E, Heinzmann A, Traherne JA, Bhattacharyya S, Leaves NI, et al (2001): Extent and distribution of linkage disequilibrium in three genomic regions. *Am J Hum Genet* 68:191–197.

Braff DL, Geyer MA (1990): Sensorimotor gating and schizophrenia. Human and animal model studies. *Arch Gen Psychiatry* 47:181–188.

Bunney WE, Bunney BG (2000): Evidence for a compromised dorsolateral prefrontal cortical parallel circuit in schizophrenia. *Brain Res Rev* 31:138–146.

Chisholm A, Tessier-Lavigne M (1999): Conservation and divergence of axon guidance mechanisms. *Curr Opin Neurobiol* 9:603–615.

Chua SE, Murray RM (1996): The neurodevelopmental theory of schizophrenia: Evidence concerning structure and neuropsychology. *Ann Med* 28: 547–555.

Clayton D (1999): A generalization of the transmission/disequilibrium test for uncertain-haplotype transmission. *Am J Hum Genet* 65:1170–1177.

Clayton D, Jones H (1999): Transmission/disequilibrium tests for extended marker haplotypes. *Am J Hum Genet* 65:1161–1169.

Dudbridge F (2003): Pedigree disequilibrium tests for multilocus haplotypes. *Genet Epidemiol* 25:115–121.

Geyer MA, Krebs-Thomson K, Braff DL, Swerdlow NR (2001): Pharmacological studies of prepulse inhibition models of sensorimotor gating deficits in schizophrenia: A decade in review. *Psychopharmacology* 156:117–154.

Ishii N, Wadsworth WG, Stern BD, Culotti JG, Hedgecock EM (1992): UNC-6, a laminin-related protein, guides cell and pioneer axon migrations in *C. elegans*. *Neuron* 9:873–881.

Jessell TM (2000): Neuronal specification in the spinal cord: Inductive signals and transcriptional codes. *Nat Rev Genet* 1:20–29.

Kaufman CA, Suarez B, Malaspina D, Pepple J, Svrakic D, Markel PD (1998): NIMH genetic initiative millennium schizophrenia consortium: Linkage analysis of African-American pedigrees. *Am J Med Genet* 81:282–289.

Keks NA, Hill C, Opeskin K, Copolov DL, Dean B: Psychiatric diagnosis after death: The problems of accurate diagnosis from the case history review and relative interviews. In: Dean B, Kleinman JE, Hyde TM, editors. *Using CNS Tissue in Psychiatric Research*. Amsterdam: Harwood Academic Press, 19–37.

Lewontin RC (1988): On measures of gametic disequilibrium. *Genetics* 120: 849–852.

Lewis CM, Levinson DF, Wise LH, DeLisi LE, Straub RE, Hovatta I, et al (2003): Genome scan meta-analysis of schizophrenia and bipolar disorder, part II: Schizophrenia. *Am J Hum Genet* 73:34–48.

Lewis DA, Levitt P (2002): Schizophrenia as a disorder of neurodevelopment. *Ann Rev Neurosci* 25:409–432.

Lewis DA, Lieberman JA (2000): Catching up on schizophrenia: Natural history and neurobiology. *Neuron* 28:325–334.

Lin JC, Ho WH, Gurney A, Rosenthal A (2003): The netrin-G1 ligand NGL-1 promotes the outgrowth of thalamocortical axons. *Nat Neurosci* 6:1270–1276.

Marenco S, Weinberger DR (2000): The neurodevelopmental hypothesis of schizophrenia: Following a trail of evidence from cradle to grave. *Dev Psychopathol* 12:501–527.

Martin ER, Monks SA, Warren LL, Kaplan NL (2000): A test for linkage and association in general pedigrees: The pedigree disequilibrium test. *Am J Hum Genet* 67:146–154.

Martin ER, Bass MP, Kaplan NL (2001): Correcting for a potential bias in the pedigree disequilibrium test. *Am J Hum Genet* 68:1065–1067.

Nakajima T, Jorde LB, Ishigami T, Umemura S, Emi M, Lalouel JM, et al (2002): Nucleotide diversity and haplotype structure of the human angiotensinogen gene in two populations. *Am J Hum Genet* 70:108–123.

Nakashiba T, Ikeda T, Nishimura S, Tashiro K, Honjo T, Culotti JG, et al (2000): Netrin-G1: A novel glycosyl phosphatidylinositol-linked mammalian netrin that is functionally divergent from classical netrins. *J Neurosci* 20: 6540–6550.

Nakashiba T, Nishimura S, Ikeda T, Itohara S (2002): Complementary expression and neurite outgrowth activity of netrin-G subfamily members. *Mech Dev* 111:47–60.

Nishimura S, Seki K, Watanabe A, Niimi K, Yoshikawa T, Nakashiba T, et al (2004): Axonal netrin-G1 regulates NMDA-receptor dependent synaptic functions in selected neural circuits. *Abstr Soc Neurosci 723:19.*

O'Connell JR, Weeks DE (1998): PedCheck: A program for identification of genotype incompatibilities in linkage analysis. *Am J Hum Genet* 63:259–266.

Serafini T, Kennedy TE, Galko MJ, Mirzayan C, Jessell TM, Tessier-Lavigne M (1994): The netrins define a family of axon outgrowth-promoting proteins homologous to *C. elegans* UNC-6. *Cell* 78:409–424.

Sham PC, Curtis D (1995): An extended transmission/disequilibrium test (TDT) for multi-allele marker loci. *Ann Hum Genet* 59:323–336.

Tessier-Lavigne M, Goodman CS (1996): The molecular biology of axon guidance. *Science* 274:1123–1133.

Torrey EF, Webster M, Knable M, Johnston N, Yolken RH (2000): The Stanley Foundation brain collection and Neuropathology Consortium. *Schizophrenia Res* 44:151–155.

Weinberger DR (1987): Implications of normal brain development for the pathogenesis of schizophrenia. *Arch Gen Psychiatry* 44:660–669.

Wong AH, Van Tol HH (2003): Schizophrenia: From phenomenology to neurobiology. *Neurosci Biobehav Rev* 27:269–306.

Yamada K, Iwayama-Shigeno Y, Yoshida Y, Toyota T, Itokawa M, Hattori E, et al (2004): Family-based association study of schizophrenia with 444 markers and analysis of a new susceptibility locus mapped to 11q13.3. *Am J Med Genet* 127B:11–19.

Yin Y, Miner JH, Sanes JR (2002): Laminets: Laminin- and netrin-related genes expressed in distinct neuronal subsets. *Mol Cell Neurosci* 19:344–358.

Zhao JH, Sham PC, Curtis D (1999): A program for the Monte Carlo evaluation of significance of the extended transmission/disequilibrium test. *Am J Hum Genet* 64:1484–1485.

Appendix 1. PCR Primers Used to Search for Nucleotide Variants in *NTNG1* and *NTNG2*

Region	Exon Length (bp)	Primers	Product Size (bp)	3′ End of Primer
NTNG1				
Exon 2	771	(F) 5′-TGCTTTATATTGCATCAGACCTC-3′	480	−603 (intron 1)
		(R) 5′-GACCTCAAAGCAGATCCCAAAA-3′		−167 (exon 2)
		(F) 5′-AGTATGTTAGGCTTCCACCAA-3′	568	−218 (exon 2)
		(R) 5′-GTCTTCACACTCACCACATC-3′		+309 (intron 2)
Exon 3	641	(F) 5′-TAGGGCAAATAAAAATGA-3′	584	+175568 (intron 2)
		(R) 5′-AAAAACGCGAACCTGTC-3′		+176118 (exon 3)
		(F) 5′-ACGAACATGGCAGCCCTATCAG-3′	529	+175966 (exon 3)
		(R) 5′-AATGCCTTCAGAACCTACT-3′		+178445 (intron 3)
Exon 4	173	(F) 5′-GGCCTGCAAATCTATCTCTTACTA-3′	511	+246439 (intron 3)
		(R) 5′-GATGACTGAATTTTACTGAT-3′		+246858 (intron 4)
Exon 5	27	(F) 5′-TGCACCTGTATTTTGTGTGTGTGC-3′	283	+258962 (intron 4)
		(R) 5′-CCTATTACATCAGAAATGGACACT-3′		+259198 (intron 5)
Exon 6	66	(F) 5′-AATTGCTTGCTCTTGTT-3′	347	+269832 (intron 5)
		(R) 5′-TTTCAAAGACATAGCATTCAT-3′		+270142 (intron 6)
Exon 7	60	(F) 5′-CTTAATTTAGGGCTACTTTTCA-3′	254	+272404 (intron 6)
		(R) 5′-TACACTTCACAGATATTCCAGATT-3′		+272813 (intron 7)
Exon 8	168	(F) 5′-ATGCCATTCCACCGTCTTT-3′	406	+282063 (intron 7)
		(R) 5′-AGGATATTTTCTACATTGAG-3′		+282431 (intron 8)
Exon 9	135	(F) 5′-TCATTAATGGACATCTTT-3′	352	+287968 (intron 8)
		(R) 5′-GGATCTTTTTCTGCTCTGA-3′		+288282 (intron 9)
Exon 10	1404	(F) 5′-GGCTGAAAACATGATGTACCAGATG-	453	+331947 (intron 9)
		(R) 5′-AGGCCTTCTTAGTTTGTACACTGTC-		+332351 (exon 10)
NTNG2				
Exon 2	698	(F) 5′-GTTTGCAAAGCTTCAGTGCTCG-3′	432	−133 (intron 1)
		(R) 5′-CAAGGATCTCCTCCAGACCTCCT-3′		+257 (intron 2)
Exon 3	644	(F) 5′-ACAGAGCAGGTTTCTCGGTTCG-3′	494	+31048 (intron 2)
		(R) 5′-GAGTACTCCTCGGTGCAGAGCA-3′		+31499 (exon 3)
		(F) 5′-CTGGCAGCCCTACCAGTTCTA-3′	469	+31421 (exon 3)
		(R) 5′-ACCAGGTAACATCCCAGGTATC-3′		+31848 (intron 3)
Exon 4	173	(F) 5′-GGAATCAAGGAGTTTCTGGCCT-3′	418	+59870 (intron 3)
		(R) 5′-ATCCACAGCTCCTGGGATTGA-3′		+60248 (intron 4)
Exon 5	24	(F) 5′-CACCCCCGTCCCCACAC-3′	320	+63577 (intron 4)
		(R) 5′-GGCCCAAGTCCCAGAGG-3′		+63864 (intron 5)
Exon 6	168	(F) 5′-CCTGGGGTGAGTCCTTCC-3′	273	+72205 (intron 5)
		(R) 5′-TGCCGTGTCCGTGCCCTCTC-3′		+72435 (intron 8)
		(F) 5′-AACCGCTGCAGCTACATTGA-3′	247	+72316 (exon 6)
		(R) 5′-ACAGTCTCCCCAGGTGATTCT-3′		+72523 (intron 6)
Exon 7	135	(F) 5′-AGTCTTCTCTCCAGGCCTGGCCA-3′	444	+73900 (intron 6)
		(R) 5′-TCTTGCTAGGCCCAGTCCACC-3′		+74301 (intron 7)
Exon 8	2659	(F) 5′-AGCCTCCTACATCCCCGGCCCA-3′	489	+75766 (intron 7)
		(R) 5′-GCCCTGCTGAGTAGCACCTGGGA-3′		+757167 (exon 8)

Nucleotide positions are counted from A of the start codons on the genomic stretches of *NTNG1* (GenBank accession No. NM_014917) and *NTNG2* (NM_032536). F, forward; R, reverse.

European Journal of Neuroscience, Vol. 20, pp. 2909–2916, 2004

Fez1 is layer-specifically expressed in the adult mouse neocortex

Kiyoshi Inoue,[1] Toshio Terashima,[2] Toru Nishikawa[3] and Toru Takumi[1]
[1]Osaka Bioscience Institute, Suita, Osaka 565-0874, Japan
[2]Department of Anatomy and Neurobiology, Kobe University Graduate School of Medicine, Kobe 650-0017, Japan
[3]Division of Psychiatry and Behavioural Sciences, Tokyo Medical and Dental University Graduate School, Tokyo 113-8519, Japan

Keywords: cerebral patterning, *in situ* hybridization, microarray, pyramidal neuron, zinc-finger

Abstract

The mammalian cerebral neocortex occupies the largest area of the cerebral cortex and is cytoarchitectually composed of six layers (I–VI). Recent molecular analysis has begun to reveal the existence of various developmental programs, including the genetic regulation of arealization of the neocortex. Although an increasing number of molecular determinants of the developmental stages of the neocortex have been identified, no genes specifically expressed in the adult neocortex have been identified to date. By global screening using microarrays, combined with systematic *in situ* hybridization, we identified a zinc-finger type transcription factor, Fez1, which is expressed predominantly in the mouse adult neocortex. No other genes in the neocortex have been shown to date to have their expression with such high specificity. Using two-color *in situ* hybridization, we show that Fez1 is mainly expressed in cortical layers V and VI, not in γ-aminobutyric acid neurons but in pyramidal neurons, the projection neurons of the cerebral cortex. Immunohistochemistry also shows that Fez1 is expressed in deep layers of the neocortex. Fez1 will be invaluable not only for the molecular understanding of corticogenesis but also for understanding the physiological functions of the adult neocortex, as well as for the use of its promoter in gene-manipulated animals and in conditional expression systems.

Introduction

The cerebral neocortex occupies the largest region of the mammalian telencephalon. Its volume evolutionally increases in relation to complexity of cognitive behavior and, thus, the proportion of the neocortex to the brain is the highest in humans among all organisms. Much of modern neuroscience has been directed towards understanding the functions and disorders of the human cortex (Kandel *et al.*, 2000). The neocortex, concerned with cognitive functioning, is composed of an enormous number of neurons and has six layers (I–VI). The majority of cortical neurons are pyramidal cells found in all layers except layer I. These pyramidal cells are the projection neurons that utilize the excitatory neurotransmitters glutamate and aspartate (Chan *et al.*, 2001). The remaining neurons that are scattered in all layers are interneurons which utilize the inhibitory γ-aminobutyric acid (GABA) and neuropeptides. Information in the neocortex is processed across the layers via an interconnected set of neurons called columns. Many neurological diseases including mental illnesses are due to the dysfunction of the neocortex.

Brain regionalization and cerebral patterning are intriguing issues, and two classical models, the protomap model (Rakic, 1988) and the protocortex model (O'Leary, 1989), have dominated research into the development of the cortical area map. The former theory is based on the idea that intrinsic regional differences are established within the neuroepithelium by molecular determinants that regulate neocortical areal specification, including the targeting of thalamic axons. The latter one is based on the idea that regionalization is induced by extrinsic cues, in particular by incoming thalamic axons, which convey positional and functional specification. Recent molecular biological techniques have begun to unveil the complex development of the cerebral cortex and its mechanism (O'Leary & Nakagawa, 2002; Garel *et al.*, 2003; Grove & Fukuchi-Shimogori, 2003). For example, the graded expression of the transcription factors, Emx2 and Pax6, in the neuroepithelium was found to be responsible for the formation of neocortical areas with the correct size proportion. Furthermore, the graded expression of these transcription factors was found to be sufficient to stably activate morphogenesis of the cerebral cortex and to repress that of adjacent structures, such as the striatum (Muzio *et al.*, 2002). The isolation and characterization of regionally expressed genes have provided useful markers and candidates for genes that may control tissue- or region-specific identity (Chenn *et al.*, 1997). Many molecular determinants including the above required for the development of the neocortex have been reported; however, no genes expressed specifically in the adult neocortex have been reported so far.

Identification of a neocortex-specific gene is important not only because it may play a key role in the development or physiological functioning of the cerebral neocortex, but also because its promoter region can be used to control neocortex-specific expression of any kind of genes of interest. Two kinds of promoters, CaMKIIα and Emx1, have been used to date for the creation of transgenic mice which express the transgene predominantly in the neocortex. However, the expression of both of these promoters is not strictly confined to the neocortex. Besides the neocortex, CaMKIIα is widely expressed in the forebrain, and strongly in the hippocampus and striatum (Erondu & Kennedy, 1985; Burgin *et al.*, 1990). Although Emx1 is expressed more specifically in the cerebral cortex than CaMKIIα, strong expression is observed in the hippocampus and the olfactory bulb as well as in peripheral tissues such as the kidney (Briata *et al.*,

Correspondence: Dr T. Takumi, as above.
E-mail: takumi@obi.or.jp

Received 24 April 2004, revised 18 August 2004, accepted 22 September 2004

doi:10.1111/j.1460-9568.2004.03763.x

1996). As described above, no genes have previously been identified that are specifically expressed in the neocortex.

Here we describe Fezl, a putative transcription factor containing zinc-finger motifs, which we identified through a microarray analysis of genes that are primarily expressed in the adult neocortex, combined with systematic *in situ* hybridization. Although slight mRNA expression was seen in the hypothalamus, the expression of Fezl is highly enriched in the cerebral neocortex. Using two-color double-labeling *in situ* hybridization, we show that Fezl is exclusively expressed in cortical layers V and VI, and its expression is not restricted to GABA neurons, but pyramidal neurons, the projection neurons of the cerebral cortex.

Materials and methods

Identification of Fezl

Young adult mice (C57BL/6N) were killed humanely by cervical dislocation, and their brains were removed and separated into the neocortex and the rest of the brain regions, immediately frozen in liquid nitrogen, and stored at −70 °C. Total RNA was extracted from individual tissues using Trizol (GibcoBRL) and poly $(A)^+$ RNA was isolated using the μMACS mRNA Isolation Kit (Miltenyi Biotec GmbH). Five micrograms of poly $(A)^+$ RNA was used for analysis with the Affymetrix Murine 6500 array and Mu 19K (subsets A, B and C) oligonucleotide arrays (Takumi *et al.*, in preparation). Twenty-nine (0.15%) mouse ESTs and 22 (0.34%) known genes, which were expressed at least fivefold (in the case of Mu 19K) and 2.5-fold (in the case of Murine 6500) higher in the neocortex than in the rest of the brain regions, were chosen for second screening using systematic *in situ* hybridization. Of the 39 candidate genes, Fezl was found to be expressed exclusively in the cortex. All protocols of experiments using animals in this study were approved by the OBI (Osaka Bioscience Institute) Animal Research Committee.

In situ *hybridization*

Adult and postnatal day 0 and 7 male mice and embryonic ICR mice purchased from Japan SLC (Hamamatsu, Japan) were used after being anesthetized with 0.1 mg/g pentobarbital sodium. Template DNAs for probes were synthesized by polymerase chain reaction (PCR) using specific primers and mouse brain cDNA or plasmids provided by RIKEN (The RIKEN Genome Exploration Research Group Phase II Team and the FANTOM Consortium, 2001). For Fezl, ^{35}S-labeled, digoxigenin (DIG)-labeled RNA probes were synthesized by *in vitro* transcription using two independent sequences (the sequence corresponding to the nucleotides 357–914 and 1449–1805) as templates. In addition, sense probes for each of the templates were synthesized as negative controls.

For the ^{35}S-labeled probes, brains were freshly frozen and 16-μm cryosections were fixed in 4% paraformaldehyde in 0.1 M phosphate buffer (PB) pH 7.4, treated with proteinase K (10 μg/mL) for 2 min and postfixed in the same fixative, acetylated with acetic anhydride, dehydrated in ascending alcohol series and air-dried. The sections were incubated for 12 h at 55 °C in hybridization buffer (50% formamide, 0.3 M NaCl, 20 mM Tris–HCl, 10% dextran sulfate, 1 × Denhardt's solution, 500 μg/mL yeast tRNA, 20 mM dithiothreitol and 200 μg/mL herring sperm DNA) containing one of the ^{35}S-labeled cRNA probes. After hybridization, sections were washed with 50% formamide/2 × standard sodium citrate (SSC) at 65 °C and incubated with 1 μg/mL RNase A in RNase buffer (0.5 M NaCl, 10 mM Tris–HCl, 1 mM EDTA pH 8.0) for 30 min at 37 °C. After rinsing with RNase buffer, sections were washed in 50% formamide/2 × SSC at 65 °C, rinsed with 2 × SSC and 0.1 × SSC, dehydrated in alcohol and air-dried. The slides were exposed to Kodak BioMax MR film for 1 week. Films were developed, and black and white images of mRNA expression were obtained. The slides were then coated with Kodak NTB-2 emulsion diluted 1 : 1 with water. Sections were exposed at 4 °C for 4 weeks, developed in Kodak D-19 and counterstained with hematoxylin.

Immunohistochemistry

Male adult ICR mice weighing 25–35 g were deeply anesthetized with 0.1 mg/g sodium pentobarbital and were perfused transcardially with PBS, followed by 4% paraformaldehyde and 0.2% picric acid in 0.1 M PB. After perfusion, the brains were postfixed for 6 h at 4 °C in the same fixative and were transferred to 20% sucrose in 0.1 M PB for 48 h at 4 °C, then were sectioned on a freezing microtome at 50 μm. The slices were stored in PBS containing 0.02% sodium azide at 4 °C until used. Free-floating sections were washed with PBS to remove any sodium azide and were incubated with Fezl antibody raised against the peptide CTATPSAKDLARTVQS (Immuno-Biological Laboratories, Fujioka, Japan), which is diluted at a ratio of 1 : 300 in 0.1 M PBS containing 0.2% Triton-X100, 5% normal goat serum for 24 h at 4 °C. The sections were then washed three times in PBS, followed by 4 h incubation with fluorescent-conjugated secondary antibody (Alexa 568 goat anti-rabbit, Molecular Probe, 1 : 1000 in 0.1 M PBS containing 0.2% Triton-X100, 5% normal goat serum) at room temperature and were rinsed with PBS and mounted onto slides using an anti-fade mounting medium (Vectashield, VECTOR).

Two-color double-labeling in situ *hybridization*

For two-color double-labeling *in situ* hybridization, a DIG-labeled Fezl probe and biotin-labeled GAD67 or CaMKIIα probes were used. Mice were perfused with 4% paraformaldehyde/PB and their brains were immersed in fixative for 8 h and in 30% sucrose/PB for 2 days. Ten-micrometre cryosections were fixed in 4% paraformaldehyde/PB, treated with proteinase K (5 μg/mL) for 2 min and washed with 2 mg/mL glycine/PBST (phosphate-buffered saline, 0.1% Tween-20). The sections were then postfixed in 4% paraformaldehyde/0.2% glutaraldehyde/PBST. The sections were incubated with prehybridization buffer (50% formamide, 5 × SSC pH 4.5, 50 μg/mL yeast tRNA, 1% SDS and 50 μg/mL heparin) at 70 °C for 1 h and with prehybridization buffer containing 500 ng/mL DIG-labeled and biotin-labeled probes at 70 °C overnight. The sections were then washed with Solution I (50% formamide, 5 × SSC pH 4.5, 1% SDS) at 70 °C, and Solution III (50% formamide, 2 × SSC pH 4.5) at 65 °C. The hybridization signal of the biotin-labeled probe was first visualized using an alkaline phosphatase conjugated anti-biotin antibody (Roche) at 1 : 2000 dilution in 1% sheep serum/TBST (Tris-buffered saline, 0.1% Tween-20), and developed with HNPP (2-hydroxy-3-naphotic acid-2′-phenylanilide phosphate)/FastRed TR (4-chloro-2-methylbenzenediazonium hemi-zinc chloride salt, Roche). The sections were observed by fluorescence microscopy and photographed. The alkaline phosphatase activity of the alkaline phosphatase-conjugated anti-biotin antibody was then abolished by treatment with 100 mM glycine/HCl pH 2.2. The signal of the DIG-labeled probe was then visualized using an alkaline phosphatase-conjugated anti-DIG antibody (Roche) at 1 : 2000 dilution in the same buffer and developed with BCIP/NBT (5-bromo-4-chloro-3-indolyl-phos-